

# Chapter 1

## Introduction

### 1.1 Display Technology

Since the last decade of the 20th century, display technology has been progressing rapidly. With the popularization of computer, internet and wireless communication, multimedia application display devices and tremendous information interchange become parts of our live, and the demand of technologies of displaying mass information in pictures and contents are getting imperative. Electronic displays are key elements to facilitate information presentations. As an interface between human being and information devices, electronic displays are demanded to process sufficient information content and be operated in various applications with different criteria, such as high resolution, high contrast ratio, high brightness, high readability, wide viewing angle, fast response time, portability, and high tolerance of environment variations. To satisfy the different demands, diverse display technologies have been demonstrated in the past years.

Cathode Ray Tubes (CRTs) were superior in all aspects in terms of electronic display device, except for its size, and power consumption. Although the CRTs techniques have developed maturely, scientists and engineers are continuously making breakthroughs to produce brighter displays, such as liquid crystal displays (LCDs), plasma display panels (PDPs), electroluminescent (EL) displays, and light emitting diode (LED) displays [1] with flatness, wider viewing angles, and full-color capability, yet, at low cost.

So far, LCD is the most successful display among these various alternatives to CRTs. LCD has the desired features of thin format, compact size, light weight, low power consumption, and high image quality. All these desired properties of LCD can fulfill the requirements of the applications including mobile phones, PDA (personal digital assistant), notebook, portable information apparatuses, digital camera, etc. With the developments of these various applications, LCDs have become the most important information displays in the near future as the role of CRTs in the twentieth century.

## 1.2 Liquid Crystal Display

Liquid crystal display [2] does not emit light itself, unlike a CRTs display, electroluminescent (EL), and Plasma Display Panels (PDPs), etc. Therefore, a so-called transmissive type is often used as the liquid crystal display device, which equipped with an illuminator called a backlight disposed at the rear surface thereof. Thus, the amount of light from the backlight which passes through the liquid crystal panel is controlled by the liquid crystal panel in order to realize images, as shown in Fig. 1.1.

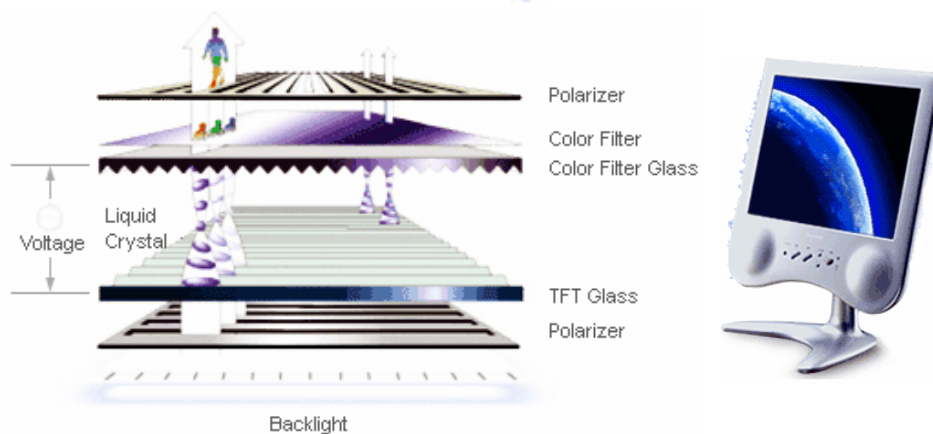


Fig. 1.1 Transmissive type LCDs

Since the liquid crystal displays of the transmissive type are advantageous in thinness · brightness · high contrast ratio and good color saturation, they have been used in various fields. However, in such a transmissive type LCD, the backlight consumes 50% or more of the total power consumption. Besides, the devices in the LCD embodiment including polarizer · pixel electrode and color filter will absorb or block the backlight. Therefore, a typical transmissive LCD device has a transmittance of about only 7.4%, as shown in Fig. 1.2, which shows a transmittance after light passes through each device of the display. The problems can be eliminated by using brighter back light, however, the power consumption is further increased. Moreover, the transmissive LCD becomes too difficult to observe under bright circumstance, which is so called “wash-out” phenomenon, for example, in direct sunlight. Therefore, transmissive type LCDs are suitable for desktop monitor instead of portable devices.

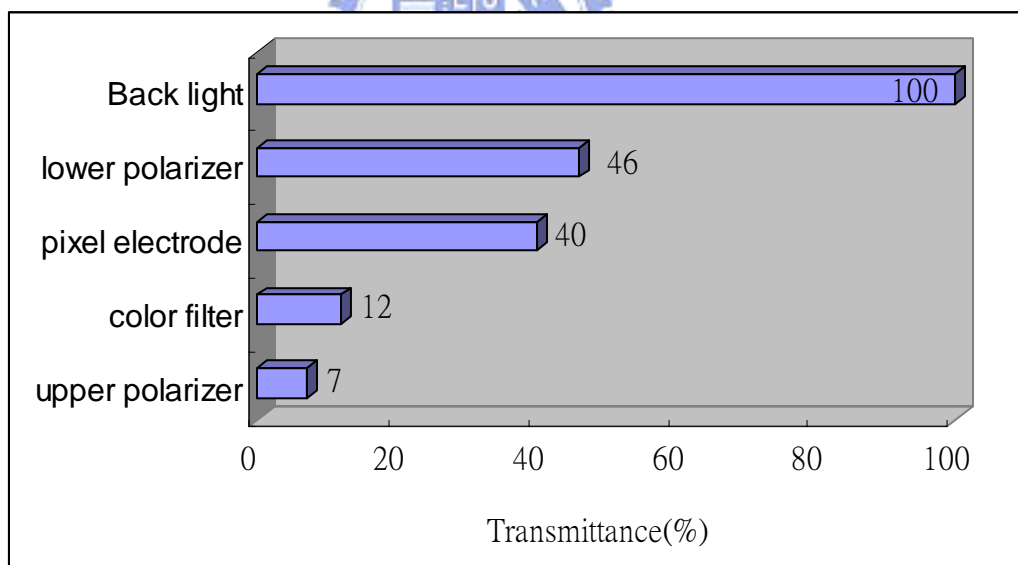


Fig. 1.2 The light luminance after light passes through each component of the LCD

In order to solve the problems in the transmissive type LCDs, a reflective type LCD [3] is proposed as shown in Fig. 1.3. The reflective type LCDs are provided with a reflector formed on one of pair of substrate in place of backlight, so that the ambient

light is reflected to show the images, thereby obtaining display light proportional to an amount of ambient light. Thus, reflective type LCDs will not wash out under bright environment and the images can be observed distinctly. Further, the reflective LCD is advantageous of light weight and low power consumption due to the elimination of the backlight. For the above reasons, the reflective LCDs are particularly suitable as the devices for the outdoor use, such as portable information terminals, and digital cameras.

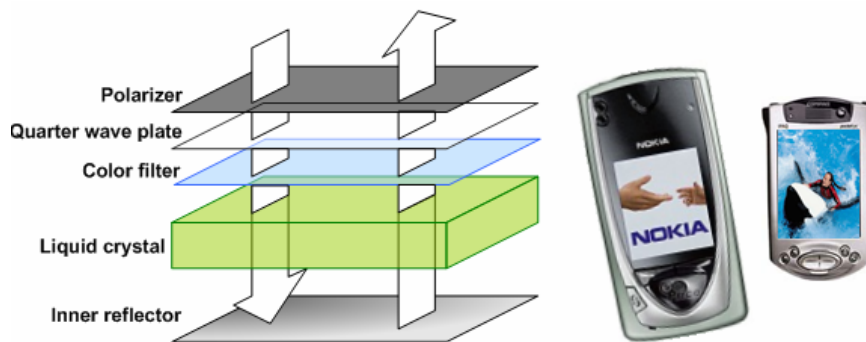


Fig. 1.3 Reflective type LCDs

However, since the reflective LCDs use the ambient light for performing the images, the display luminance particularly depends on the surrounding environment, and it always loses its visibility under dark ambient. Further, it is hard to control the purity of the ambient light, therefore, such a reflective LCD do not provide sufficiently high quality display in terms of brightness, contrast and color saturation. Accordingly, further improvement in brightness and contrast for portable devices is demanded. In order to overcome the problems of both transmissive and reflective LCDs, a construction which realizes both the transmissive and reflective mode display in one liquid crystal device has been disclosed and named transflective type LCDs, as shown in Fig. 1.4.

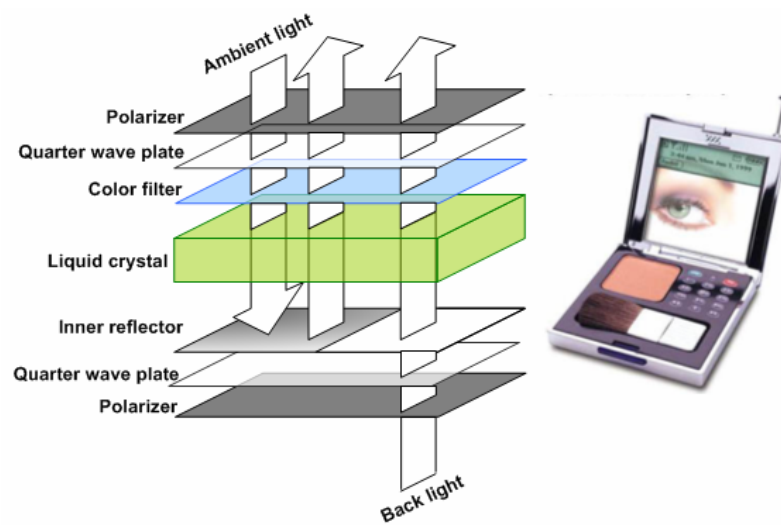


Fig. 1.4 Transmissive type LCDs

### 1.3 Transflective LCDs

The liquid crystal displays using both the transmitted light and reflected light are generally referred to transflective LCDs, which can be used under the circumstance where the ambient light is weak while maintaining the advantages of the reflective LCDs. There are several kinds of transflective LCDs: transflective LCDs with transflector device [4], single cell gap structure [5][6] and double cell gap structure [7][8][9], etc. Following the approach and characteristic of each transflective LCD will be introduced.

#### 1.3.1 Transflective LCDs with transflector device

A transflective LCD which comprises a transflector device between color filter and glass substrate is shown in Fig. 1.5. Such a transflector transmits a part of incident light and reflects the rest. During the transmissive mode, it transmits light from the backlight to be visible. On the other hand, it reflects the ambient light to perform display during the reflective mode.

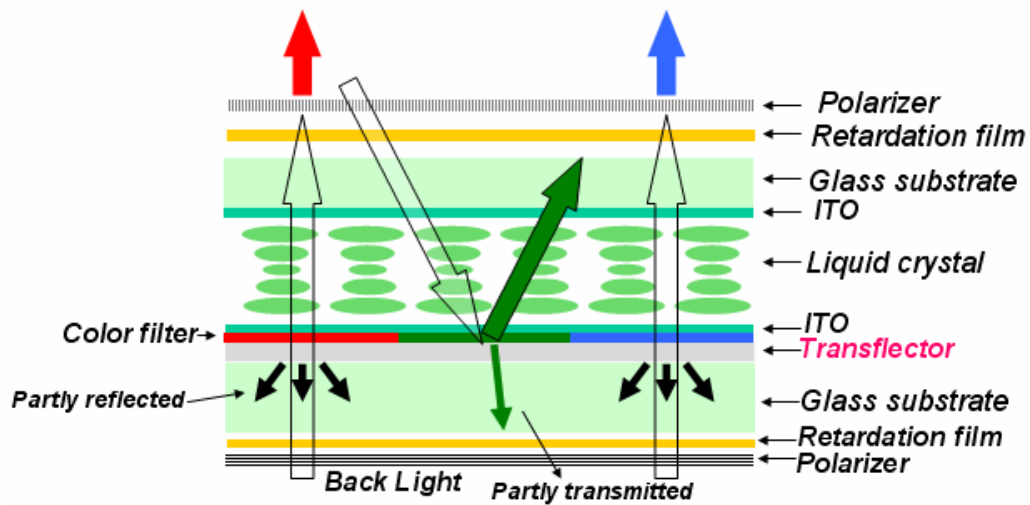


Fig. 1.5 Transfective type LCDs with translector device

Nevertheless, for a common product, the reflection of the translector is approximately 65% of the incident light. Therefore, as the display is used under transmissive mode, 65% of light will be reflected. On the other hand, under reflective mode, there exists transmitted light, at the expense the brightness and light efficiency, unless a brighter light source is chosen, which requires extra energy and reduces the lifetime of the battery. An increase of the transmission in the transmissive mode worsens the brightness and contrast in the reflective mode. As a consequence, a translector device is not a good solution for transfective LCDs.

### 1.3.2 Single-cell gap Structure

In March, 2003, Sharp corporation developed a transfective LCD using divided pixels, where a pixel is split into reflective (R) and transmissive (T) sub-pixels. Usually, the R and T area ratio is 4:1, in favor of reflective display. In a bright ambience, the incident light on the T sub-pixel is absorbed by the lower polarizer and the device works as a reflective display. In a dark ambient, the backlight transmits the T sub-pixels and the device works as a transmissive display. As implied in the name of single cell gap, the cell gap for R and T sub-pixels are the same, as shown in Fig. 1.6. The cell gap

is optimized for R sub-pixels, as a result, the light transmittance for the T mode is lower than 50% due to the light only propagating the LC layer once, and resulting in different optical difference compared with R sub-pixels. Besides, a challenge of such a transfective display is the color balance between the R and T sub pixels. For R sub-pixels, the light transverses the color filters twice. However, the light transmits color filters only once in the T sub-pixels. To have the same color saturation, the color filters in the T sub-pixels should have double pigment concentration as compared to those of the R sub-pixels; however, it increases the fabrication complexity.

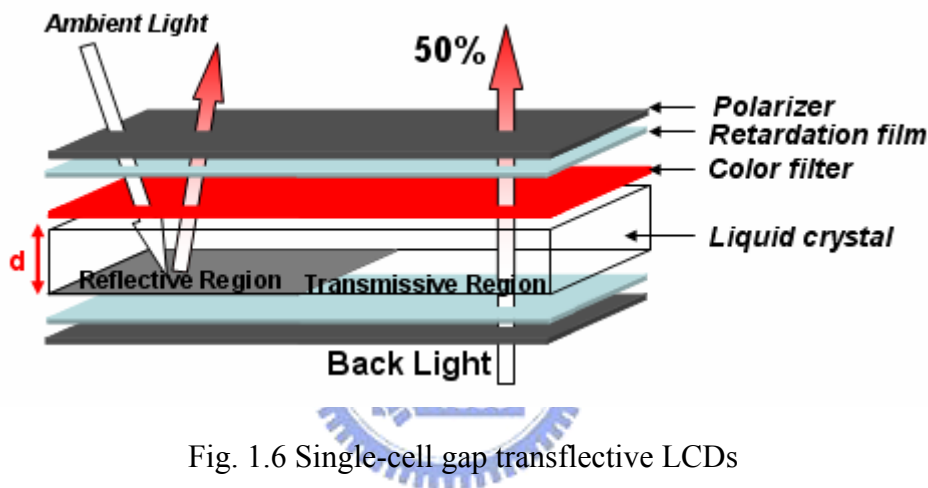


Fig. 1.6 Single-cell gap transfective LCDs

### 1.3.3 Double-Cell gap structure

In order to improve the low transmission efficiency in single-cell gap transfective LCDs, Sharp Corporation proposed a new structure named double-cell gap structure in August, 2000, where the cell gaps for R and T sub-pixels are  $d$  and  $2d$ , respectively, as shown in Fig. 1.7. As the liquid crystal in R region fulfills a  $\lambda/4$  condition, those of the liquid crystal in T region fulfills a  $\lambda/2$  condition due to its double thickness. Therefore, employing a  $\lambda/4$  retardation film between the polarizer and liquid crystal, the optical path difference in both R and T regions are the same. As a result, both R and T sub-pixels have high light efficiency.

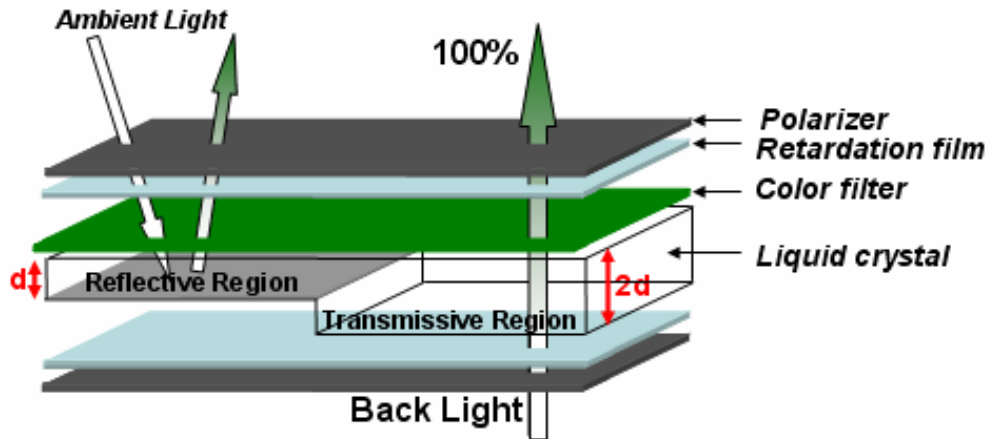


Fig. 1.7 Double-cell gap transfective LCDs

Although double cell gap structure can improve the transmission efficiency according to single cell gap structure. However, the thicker the LC layer, the slower the response time, which is roughly proportional to  $1/d^2$ . Therefore, the T sub-pixels have four times slower response time than that of the R sub-pixels, which results in inferior image quality. On the other hand, different LC layer thickness raises the complexity in fabrication due to glass etching and ITO electrodes coating on the transmission are needed. These processes are all resulted in high cost. Moreover, further improvement in the color saturation balance for T and R modes is pressingly demanded.

#### 1.4 Motivation and Objective of this Thesis

As described above, in conventional transfective liquid crystal displays, each pixel is divided into reflective and transmissive areas according to a specific rate. In bright environment, it makes use of the reflective area to reflect the ambient light to illuminate images. In dark environment, it makes use of a backlight system and then backlight passing through the transmissive area is regarded as the light source. However, when the backlight is used as the light source, the reflective area can become a block that backlight can not pass through. Therefore, in comparison with a transmissive LCD, equal light efficiency of the backlight requires a more powerful backlight system, which results in higher power consumption.



In order to solve the problem about light efficiency of the backlight in transfective LCDs, a novel structure for transfective LCD technology, micro-tube array, is proposed to improve the light efficiency. The characteristic of this design is to make use of a micro-tube structure which is similar to a funnel in shape and to allow most backlight enter this structure from larger aperture. On account of the characteristic of the funnel in structure, the incident light can be collected to smaller aperture so that light efficiency of the backlight can be increased substantially. Besides, this design is to build a micro-tube array below the reflective area in transfective LCDs. It can be fabricated exactly inside the layer which is the passivation layer of the thin film transistor (TFT). Therefore, the flat layer would be available further for increasing light efficiency of the backlight in addition to the function for flattening out.

Based on the advantage of the micro-tube array for improving light efficiency of the backlight, the transmissive area can be reduced so that the ratio of the transmissive area to the reflective one can be redistributed. This will enlarge the reflective area and make more ambient light be utilized to illuminate images. Thus, both of the backlight and ambient light can be utilized efficiently by adding the micro-tube array in a transfective LCD.

## **1.5 Organization of this thesis**

The thesis is organized as following: the principles and the features of the micro-tube array will be presented in **Chapter 2**. In **Chapter 3**, the simulated results including light efficiency, light enhancement, and various aperture shapes used to verify and optimize our design will be presented. In **Chapter 4**, the considerations of the mask design are discussed, and the fabrication technologies to realize the micro-tube array are summarized. The major measurement equipments used to characterize the fabricated the micro-tube array are illustrated. About the experimental results, several samples fabricated by designed photo-mask are demonstrated. Based on the

measurement results, several critical parameters in fabrication process are discussed, and then the desired structure will be realized and modified. The summary of the dissertation and the future works are given in **Chapter 6**.



# Chapter 2

## Principle

### 2.1 Introduction

Due to the technical challenge for the backlight system in conventional transmissive LCDs, some micro-optics components are considered to solve those problems initially. Diffractive components (Fresnel lens [10] [11] [12] and grating [13] [14] [15]), refractive component and micro-tube array are proposed and described in the following. Besides, transmissive light efficiency enhancement will be calculated to determine the capability of collecting light, respectively. The transmissive light efficiency enhancement is expected to be larger than 150% in order to set a fitting goal that would be reached.

### 2.2 Comparison of Various Micro-Optics Components

#### 2.2.1 Diffractive Component (Fresnel Lens)

First, a Fresnel lens is considered and its structure is shown in Fig. 2.1. According to the diffraction principle of the Fresnel zones, the radius of Fresnel zone can be calculated. Assuming that all of the light entering the Fresnel lens can exit from the aperture, then the light efficiency can be increased to  $(3/2.5)^2=144\%$ . However, due to the fabrication ability, the Fresnel lens only can be treated as a binary component. Thus, the first diffractive efficiency is about 35%, that the transmissive light efficiency enhancement is only about 115%. Obviously, this is not a desired result.

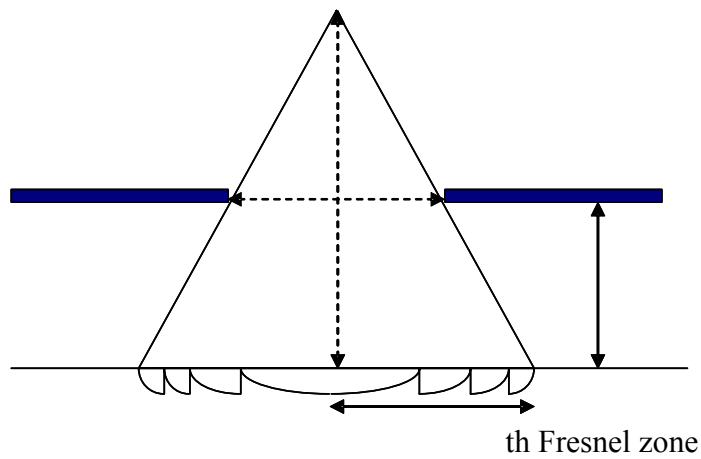


Fig. 2.1 Schematic diagram of Fresnel lens

### 2.2.2 Diffractive Component (Grating)

The structure of a grating is shown in Fig. 2.2. The diffraction angles  $\theta$  are calculated for three colors of light, Red, Green, and Blue, respectively. Here, the diffractive efficiencies of Red, Green and Blue rays are also considered on the actual condition, thus the calculated light efficiency enhancements for R, G and B rays are about 123%, 120% and 117%, respectively. This still can not achieve our target as well.

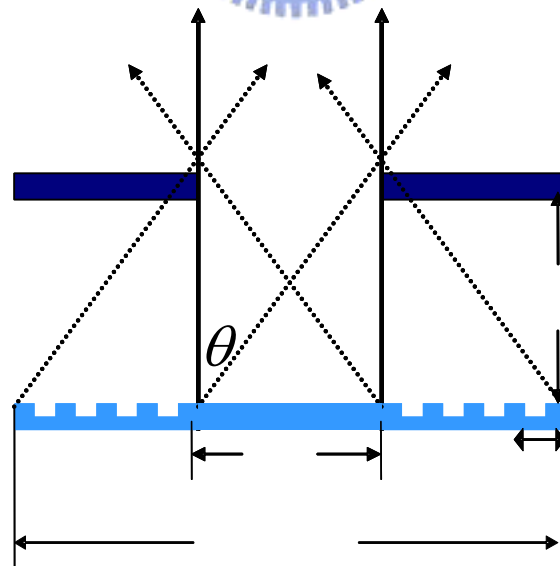
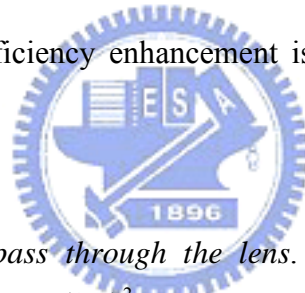


Fig. 2.2 Schematic diagram of grating

### 2.2.3 Refractive Component

Because diffractive components fall short of our expectation, two refractive components [16] are proposed based on the advantages that they have minor loss caused by diffraction effect and some limitations in fabrication process. As shown in Fig. 2.3, it is the structure of a refractive trapezoid-shaped prism. The materials with the refractive indices  $n_1$  and  $n_2$  are respectively ITO and SiO<sub>2</sub>, where  $n_1$  equals to 1.9 and  $n_2$  equals to 1.5. The refractive angle at the interface is 17.64°. Besides, it is assumed that the aperture is 5 $\mu$ m and the tilt angle is 30°. Fig. 2.3(a) illustrates the calculated structure of the lens. Furthermore, optical software is utilized to simulate the light efficiency enhancement, which is about 250% and the calculation is shown as follows. Another kind of refractive lens is shown in Fig. 2.4. Based on the similar principle of condensing light, its light efficiency enhancement is also approximated to 250% by simulation.



*Assume all backlight can pass through the lens.*

$$\text{Enhancement} = \text{area ratio} = \frac{\pi(2.5)^2}{\pi(2.5+1.59)^2} \approx 250\%$$

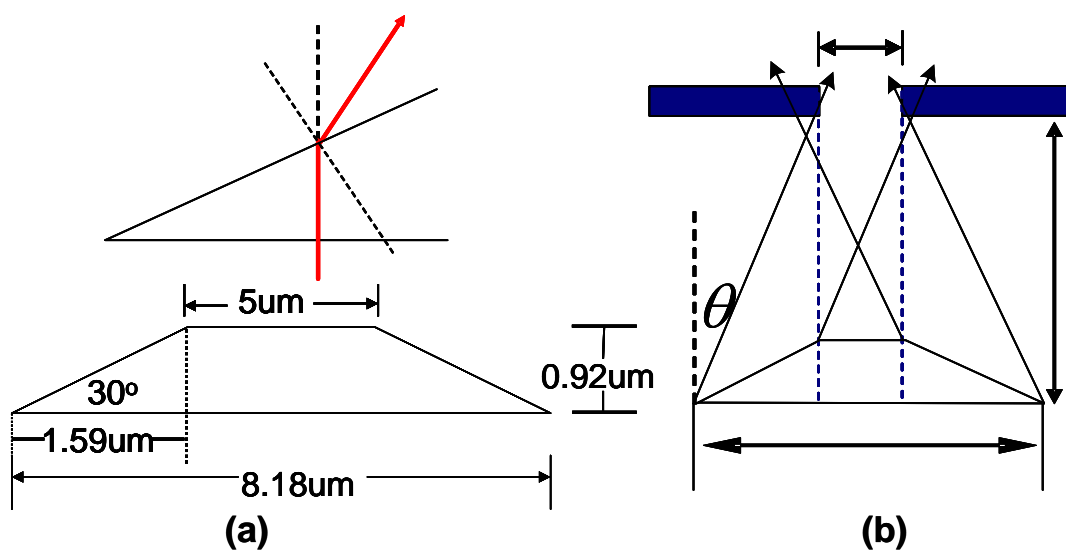


Fig. 2.3 (a) Illustration of calculating light efficiency (b) Schematic diagram of a trapezoid prism

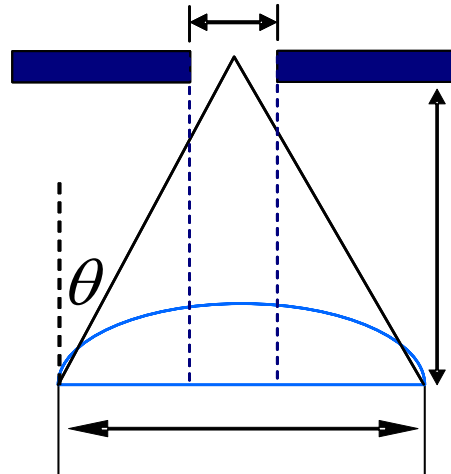


Fig. 2.4 Schematic diagram of a refractive lens

As the calculated results, the refractive components have better light efficiency enhancement. However, if the materials and fabrication process are taken into consideration, it should be noted that refractive components will have some drawbacks which are summarized as follows.

The light efficiency enhancement was calculated on condition that the materials of refractive components are completely transparent. In fact, ITO transparent electrode is used as the material because the refractive ratio of ITO is about 1.9, thus a larger refractive angle can be determined according to the Snell's Law [17]. On account of the larger refractive angle, the lens or prism doesn't require a large curvature or slope, thus, can reduce the thickness to around  $0.9\mu\text{m}$  to match conventional fabrication process. However, the absorption of ITO with  $0.9\mu\text{m}$  as calculated in Fig. 2.3(a). thickness is around 50% by using optical measurement instruments. Therefore, light efficiency enhancement will be decreased to only 125%, which is still far away to 150%.

Due to the above discussions, we conclude that the diffractive and refractive components are not appropriate to be realized. Therefore, a new micro-optics component "micro-tube array", which has simple structure, high light efficiency and compatible fabrication are proposed and be described in the following section.

## 2.3 Design of Micro-tube Array

### 2.3.1 Features of a Single Micro-tube

The achievement of this thesis is to propose a novel micro-optics component which can increase the utilization efficiency of backlight in transmissive LCDs. We proposed “Micro-tube array” structure which is composed of four main parts: the upper aperture, the lower aperture, the tube, and the high-reflecting film, as shown in Fig. 2.5.

A cross-sectional and a three-dimensional plot of a single micro-tube are shown in Fig. 2.5. Obviously, without the micro-tube structure, the available backlight is only rays R1 and R2. However, with the micro-tube, the unavailable rays R3 to R6, which are blocked, can be transmitted to exit from the upper aperture.

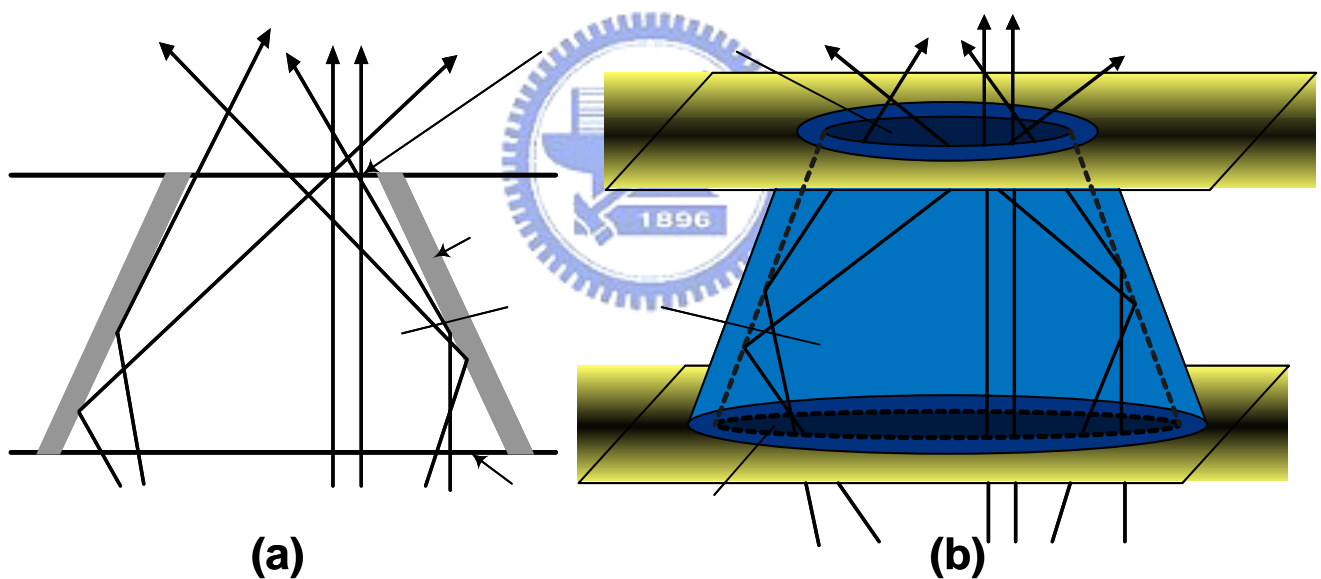


Fig. 2.5 (a) A cross-sectional view of a single micro-tube structure

(b) A 3-D picture of a single micro-tube structure

### 2.3.2 Features of Micro-tube Array

In the following discussion, we will broaden the analyses by considering a micro-tube array in order to further explain its capability of collecting. A description of the characteristic of micro-tube array is now given below.

The comparison of one sub-pixel comprising a micro-tube array with a

conventional sub-pixel in the transfective LCD is depicted in Fig. 2.6. In the conventional structure, only rays passing through the transmissive region can be utilized, thus the utilization efficiency of the backlight is only about one-fifth. (Assume the ratio of the transmissive region to the reflective region is 1:4.) Compared to the conventional structure, with the micro-tube array in a sub-pixel, almost the whole sub-pixel region can be covered with the area of the lower apertures as the dash-line circle shown in Fig. 2.6. Besides a small fraction of backlight which is blocked by the areas outside of the lower apertures and some large angle incident rays, the rest of backlight can pass through the upper aperture of micro-tube array to increase the transmissive light efficiency. Therefore, the light efficiency of backlight can be improved efficiently, and then the reflective region can be also enlarged to enhance the reflective brightness.

Furthermore, the shape and the size of an upper aperture in a micro-tube array determine a transmissive region in each sub-pixel, as shown in Fig. 2.6. Therefore, the transmissive region in a sub-pixel can be redistributed. In addition, the non-transmissive region among the upper apertures will be coated with a high-reflecting material as a reflector to be the reflective region. As a result, the brightness of the transmitted backlight and reflected ambient light can be optimized so that the whole image quality can be improved for both indoor and outdoor applications.



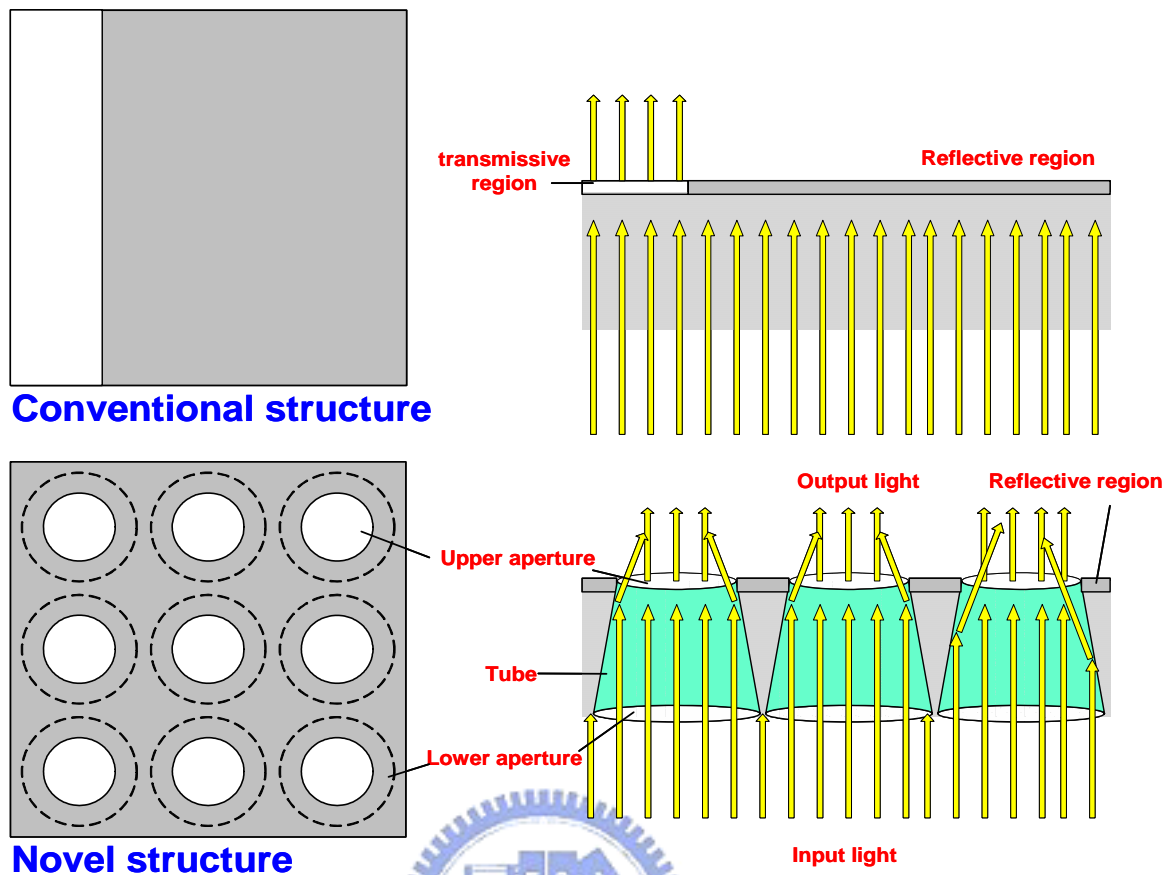


Fig. 2.6 The comparison of one sub-pixel comprising micro-tube array against a conventional one

### 2.3.3 Micro-tube Array in a Display Panel

The whole structure of a transflective LCD with a micro-tube array includes upper polarizer, upper retardation film, upper glass substrate, color filter, upper ITO, liquid crystal layer, lower ITO, reflective area, micro-tube array, thin film transistor (TFT), lower glass substrate, lower retardation film and lower polarizer, as shown in Fig. 2.7. The micro-tube array is located between lower glass substrate and lower ITO. Besides, the material utilized to fill the valley region between each micro-tube can also be the passivation layer of TFT structure. Consequently, not only the backlight but also the space in TFT layer can be efficiently utilized.

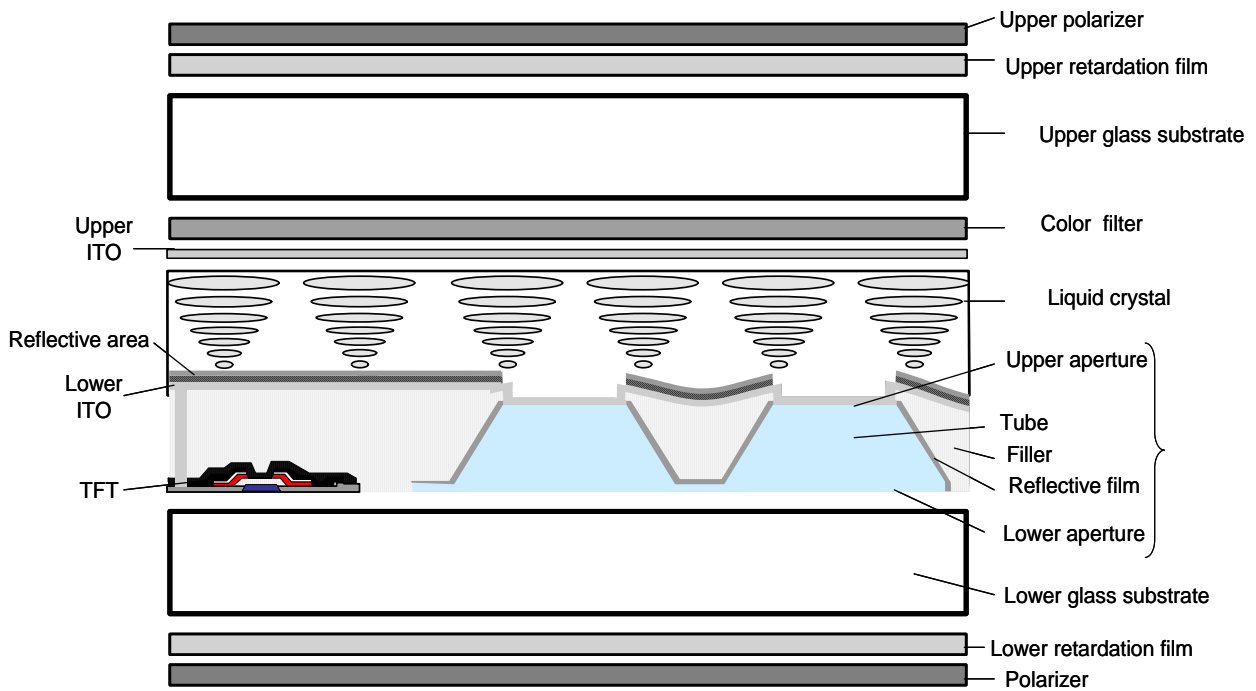


Fig. 2.7 Schematic diagram of the single cell-gap transreflective LCD with micro-tube array

## 2.4 Summary

Compared with the Fresnel lens, grating and refractive component, micro-tube array has a distinguished capability of collecting backlight. After backlight is transmitted effectively to increase the image quality by the micro-tube array, area ratio of the reflective region to the transmissive region can be redistributed so that the brightness of the reflective light can also be further enhanced. By a typical TFT-LCD process [18] [19] [20], this structure can be fabricated in a layer between lower glass substrate and lower ITO. Therefore, we can make use of the space in a panel effectively and do not need many additional fabrication steps. In the following chapter, simulation software will be utilized to further design and optimize micro-tube array structure so that the highest light efficiency enhancement can be obtained.

# Chapter 3

## Fabrication and Measurement Instruments

### 3.1 Introduction

A preliminary structure will be used to confirm the features of the micro-tube array. The embodiment including several fabrication processes will be shown in the following sections, and all the fabrication process, technologies and instruments which are available to develop such a preliminary structure will be introduced in this chapter.

First, the semiconductor fabrication process including mask generating, re-flowing, spin coating, exposure and development will be used. Besides, the characteristics and performance of the fabricated structure, such as similarity to the geometric design, light efficiency and light efficiency enhancement were measured by typical semiconductor measurement systems, such as scanning electron microscope (SEM), atomic force microscope (AFM), and ELDIM EZContrast 160R. The major features of the above mentioned instruments will be illustrated in this chapter.

### 3.2 Semiconductor Fabrication Process

In this section, we started to fabricate a prototype to characterize the features of the micro-tube array structure. However, it is difficult for us to produce a whole display panel, therefore, a prototype was utilized to measure the light efficiency and light efficiency enhancement.

The semiconductor processes including spin coating, mask generating, lithography, and development will be used to fabricate the desired structure. Usually, the semiconductor process produces the structure on silicon wafer; however, for the display applications the glass is widely used as the substrate. We implemented our fabrication

at AU.

The detailed fabrication processes are listed below and the fabrication process is shown schematically in Fig 3.1.

- (a) Substrate preparation: For the display application, the glass is widely used as a substrate. In the fabrication, the glass with about 0.7mm thick was chosen. Besides, an organic film (about 5 $\mu$ m) was taken as the material due to its easy preparation and suitability for fabrication process. Therefore, after the initial cleaning, an organic film was coated on the glass.
- (b) UV exposure with G-Line (436nm) stepper: The micro-tube array with desired depth and aperture size according to the simulation results was fabricated by using two photo masks equipped with the G-line stepper. Therefore, after the substrate preparation, the exposure of the first mask was then proceeded to transfer specific patterns which are on mask onto the organic substrate. By controlling the exposure time, and the following re-flowing procedure [21], a preliminary structure of the micro-tube array can be fabricated.
- (c) Aluminum sputtering: After hard baking the fabricated micro-tube array structure, aluminum film was sputtered on the surface of the micro-tube array by a sputter coater.
- (d) Photoresist coating: The Al-sputtered structure was spun coating with a positive photoresist.
- (e) Exposure and development: After soft baking, the exposure of the second mask, development and etching process was used to keep the photoresist above upper apertures of micro-tube array structure released.
- (f) Aluminum etching: After exposure and development, one kind of Aluminum acid was utilized to remove the aluminum layer above upper apertures of micro-tube array structure, and then the rest was kept as a reflector.

(g) Characterization: After the fabrication, the light utilization efficiency will be measured.

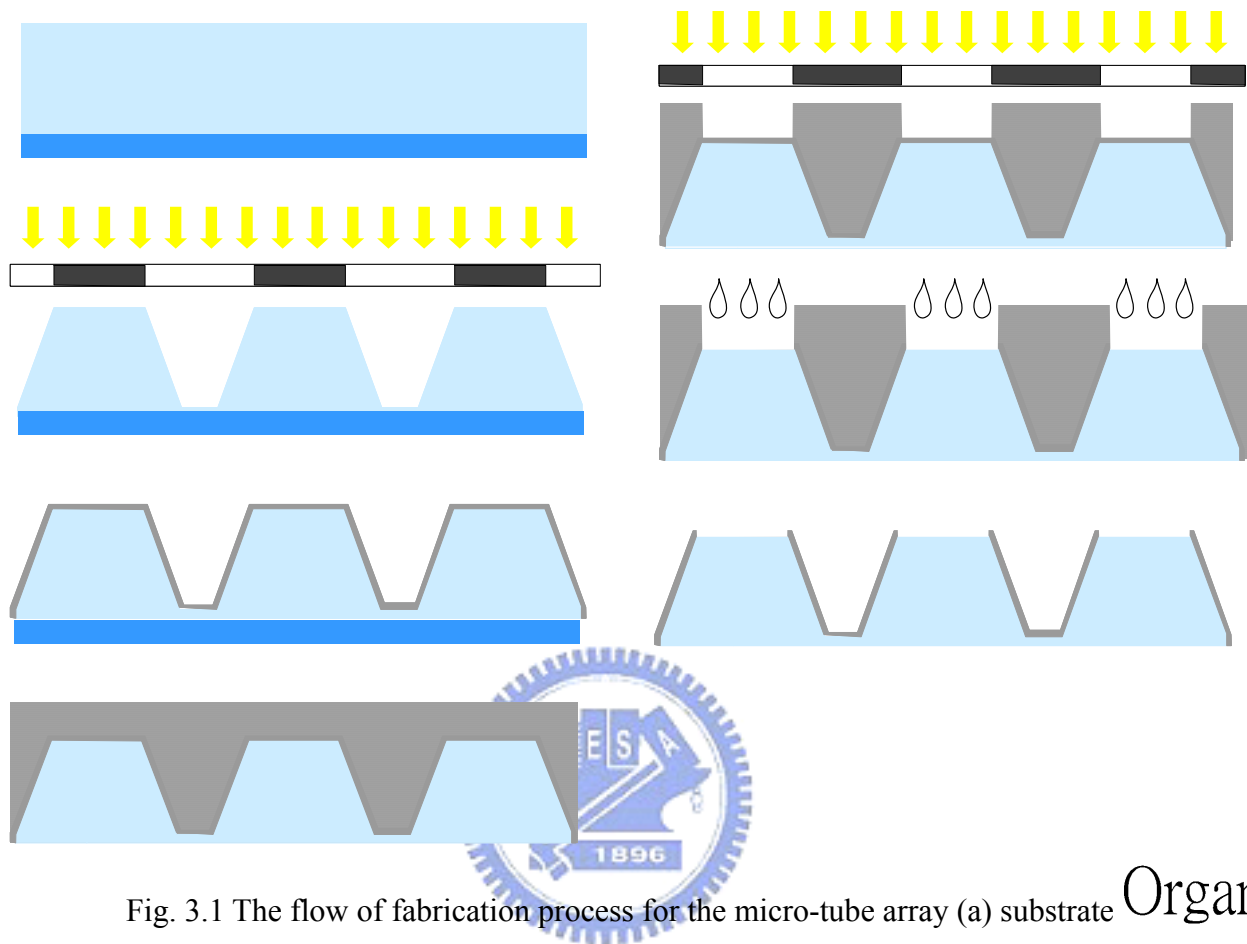


Fig. 3.1 The flow of fabrication process for the micro-tube array (a) substrate preparation (b) UV exposure (c) Al sputtering (d) photoresist coating (e) exposure and development (f) Al etching, and (g) the fabricated structure

Organic layer

Glass substrate

### 3.3 Measurement System

After the fabrication of the micro-tube array structure, the inspection will be performed to make sure that the fabricated structure agrees with the original design. Here, scanning electron microscope (SEM) and atomic force microscope (AFM) will be introduced. Besides, after the fabrication process, the measurement system is necessary. Therefore, one kind of measurement system, the ELDIM EZContrast 160R (diffuse type) will be demonstrated.

### 3.3.1 Scanning Electron Microscope (SEM)

A scanning electron microscope (SEM) is an essential instrument to measure the accuracy and fidelity of the fabricated microstructure, as shown in Fig. 3.2. It scans electrons reflecting onto a fluorescent screen across the target where the image is captured by a camera and enlarged. Electrons are much smaller than atoms, so a scanning electron microscope paints a razor-sharp image of the target, and the feature variation of few Å can be observed. This is useful for mapping details of objects that optical microscopes can not resolve. Using the electromagnetic lenses to focus the accelerated electron beam, the diameter of electron beam can be converged to the dimension of  $10^{-3}$  um. The secondary electrons are generated where the focused accelerated electrons bombard the sample. Detecting the secondary electrons can determine the location of bombardment. Simultaneously, the focusing electron beam scans the surface of sample, with the aid of scanning coil, to map the feature of measured area.



Fig. 3.2 Schematic diagram of SEM

In our work, a HITACHI S-4000 SEM was used to measure the quality of our

fabricated microstructure elements. The line width, etching depth, and aperture size can be accurately measured.

### 3.3.2 Atomic Force Microscope (AFM)

AFM consists of a sharp tip mounted on the end of a flexible cantilever spring. Forces from the sample act on the tip and generate some measurable change in the cantilever, such as deflection or shift in resonant frequency. To form an image, the interaction between the sample and tip is mapped to the monitor as a function of position mechanically scanning the sample relative to the tip in a raster pattern into the photo-detector. By detecting the difference in the photo-detector output voltages, changes in the cantilever deflection or oscillation amplitude are determined. A schematic diagram of this mechanism is depicted in Fig 3.3.

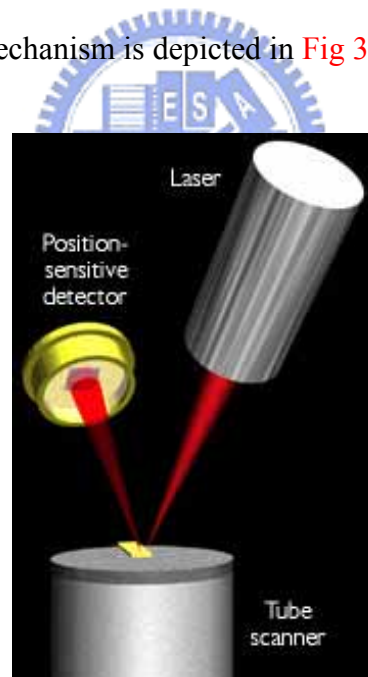


Fig. 3.3 Concept of AFM and the optical lever

There are two major operation modes for AFM:

- (a) Contact mode

Contact mode is the most common method to operate the AFM. As the term suggests, the tip and the sample remain in close contact as the scanning proceeds. One of the drawbacks of remaining in contact with the sample is that there exists a large lateral force on the sample as the tip is dragged on the specimen.

#### (b) Tapping mode

Tapping mode consists of oscillating the cantilever at its resonance frequency (typically hundreds of kilohertz) and positioned above the surface so that it only taps the surface for a very small fraction of its oscillation period. The laser deflection method is used to detect the root-mean-square (RMS) amplitude of cantilever oscillation. The advantage of tapping mode over contact mode is that it eliminates the lateral, shear forces present in contact mode, which enables tapping mode to image soft, fragile, and adhesive surfaces without damaging them.

### 3.3.3 Measurement systems

After the preliminary fabrication of the micro-tube array structure, we used a measurement instrument to measure the light utilization efficiency and light distribution.

#### 3.3.3.1 ELDIM EZContrast 160R

The ELDIM EZContrast 160R which has diffuse and collimated illumination types with a plane detector consisting of various directional CCD sensors to detect the transmissive and reflective light can be utilized to measure the luminance, contrast, color of the transfective LCDs at one time. The schematic diagram of the display measurements setup in both transmissive and reflective mode of ELDIM EZContrast 160R are as shown in Figs. 3.4 (a) and (b).



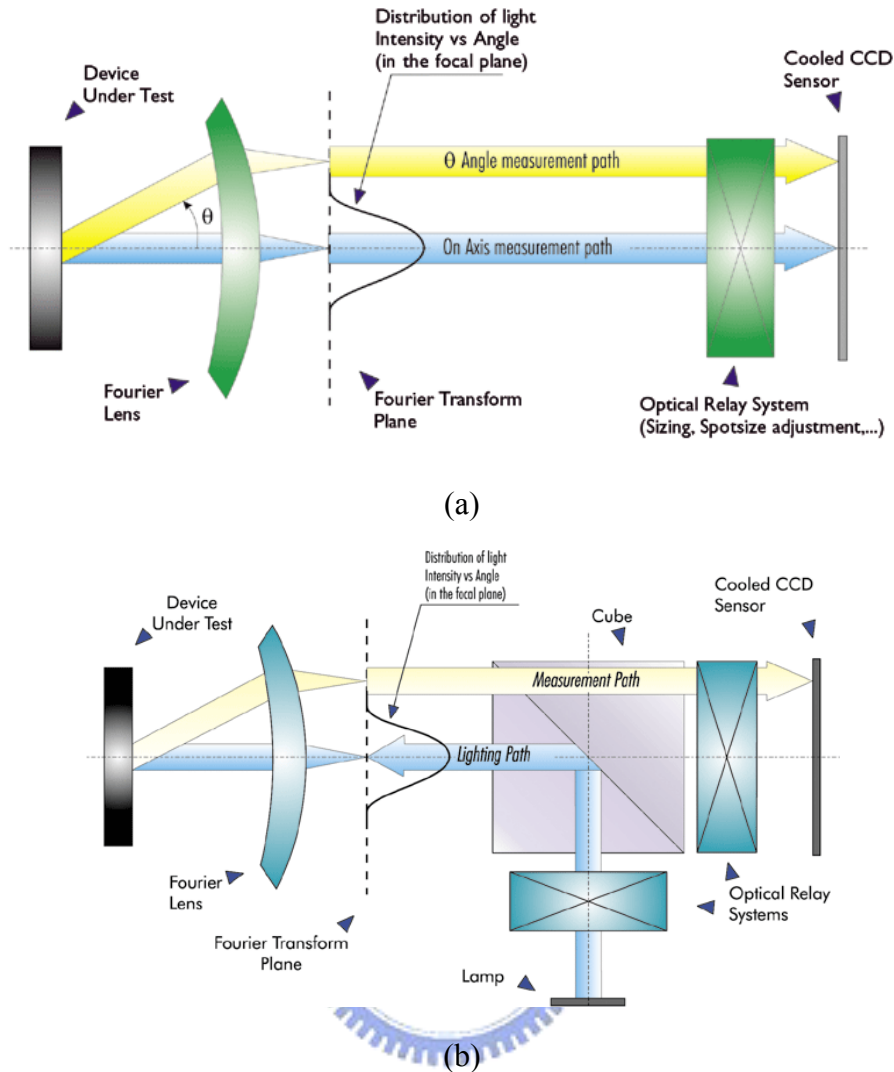


Fig. 3.4 Display measurement setup of ELDIM EZContrast 160R (a) transmissive and (b) reflective mode

The options for testing under illumination are based on the combination of Fourier Optics and cooled CCD sensor head. A suitable light source on the side of the equipment provides the illumination. As shown in Fig. 3.4 (a), the measurement is used for transmissive mode LCDs, where the first lens provides a Fourier transform image of the display surface. Every light beam emitted from the test area with a  $q$  incident angle will be focused on the focal plane at the same azimuth and at a position  $x=F(q)$ . The angular characteristics of the sample are thus measured simply and quickly, without any mechanical movement. The Optical Relay System scales the Fourier transform image

of the measured surface on the CCD sensor. The captured image is used in order to obtain, after a suitable computation, the viewing angle map of the measured display which is dependent to the display luminance with angle. On the other hand, as shown in **Fig. 3.4** (b), an optical relay system combined with a beam-splitter cube enables to conjugate the light source plane with the Fourier plane. The light source distribution function allows controlling the angular distribution of illumination. Beside, the light through the system can extend up to the viewing cone of the Fourier lens ( $\pm 80^\circ$  or  $\pm 60^\circ$ ). In our measurement, we used the collimated light, BEF II and BEF III as the backlight to analyze the luminance, light utilization efficiency and light distribution of the fabricated micro-tube array prototype.



# Chapter 4

## Simulated Results and Discussions

### 4.1 Introduction

Based on the principle described in chapter 2, we established a simulation model used to characterize the features of the transfective LCD with micro-tube array.

First, the incident angles were analyzed for a single micro-tube structure. Besides, two different kinds of commercial backlight sources were utilized to simulate the light utilization efficiency for a micro-tube array. After that, the structure of micro-tube array was designed and optimized. Further, various shapes and arrangements of the apertures were also discussed and compared. Finally, masks were designed based on the simulation results.



### 4.2 Simulation Software

The optical simulator Advanced Systems Analysis Program (ASAP™), developed by Breault Research Organization (BRO) was used to design the optimized transfective LCD structure and simulate its light efficiency and light distribution.

### 4.3 Simulation of Light Efficiency

As mentioned in chapter 2, a micro-tube array structure employed between the lower glass substrate and ITO transparent electrode is used to collect transmitted light to enhance the light efficiency of the backlight. Therefore, in this section, ASAP was used to perform the simulation, and then the structure of micro-tube array can be designed and optimized.

### 4.3.1 Analysis of Incident Angle

In order to optimize a micro-tube array, incident light at various angles must be analyzed so that the structure can transmit the highest percentage of backlight.

First, we need to develop a theoretical method for analyzing the angle of the incident light. Considering a regularly-arranged array of circular apertures, and assuming the incident light inside the tube is reflected once only on the tube wall, then a single tube was utilized to analyze the angle of incident light. If the incident light is reflected too many times on the tube sidewall, its energy (light flux) will be consequently consumed. Under this constraint, we calculated the maximum incident angle (MIA) of the light projected onto each position on the tube. If the incident angle on each location is greater than the corresponding MIA, the incident light will be reflected more than one time inside the tube. As shown in Fig. 4.1, at point C the MIA is  $\theta_{ic(max)}$ . Therefore, if the incident angle is equal to  $\theta_{ic(max)}$  or smaller, the light is reflected once only inside the tube just as R2. On the other hand, If the incident angle is greater than  $\theta_{ic(max)}$ , the light is reflected more than one time inside the tube just as R3. Herein  $\theta_{ia(max)}$  is defined as the MIA at point A. It is worth noticing that the MIA at point A will be the smallest angle compared with other points on the tube wall.

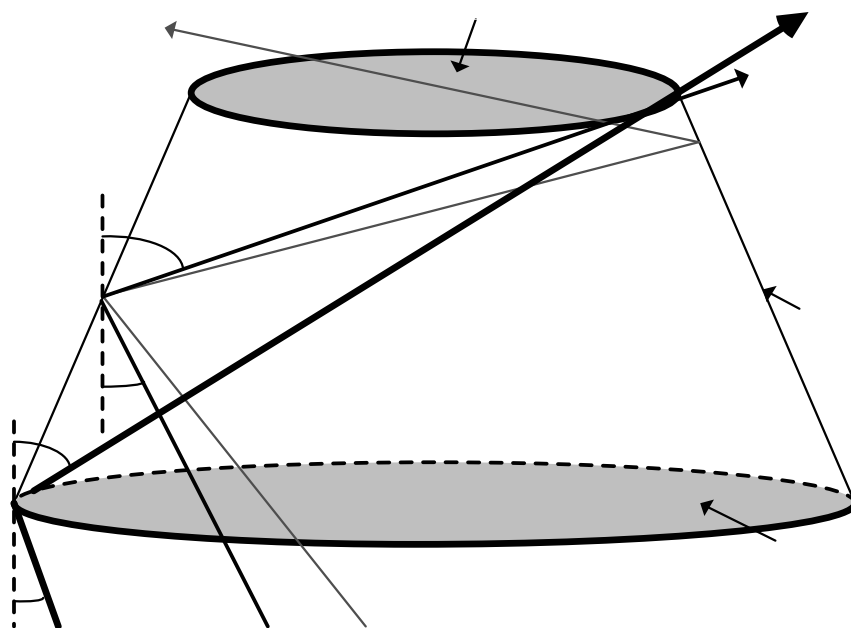


Fig. 4.1 Schematic figure of the incident light passing through the tube by only one time of reflection.

In order to make an accurate analysis, we need to define some parameters, as shown in Fig. 4.2. The diameter of the upper aperture is defined as AP, the tube depth (length) is d and the tilt angle of the tube wall is  $\theta$ . Other parameters are shown by the notations in the figure.

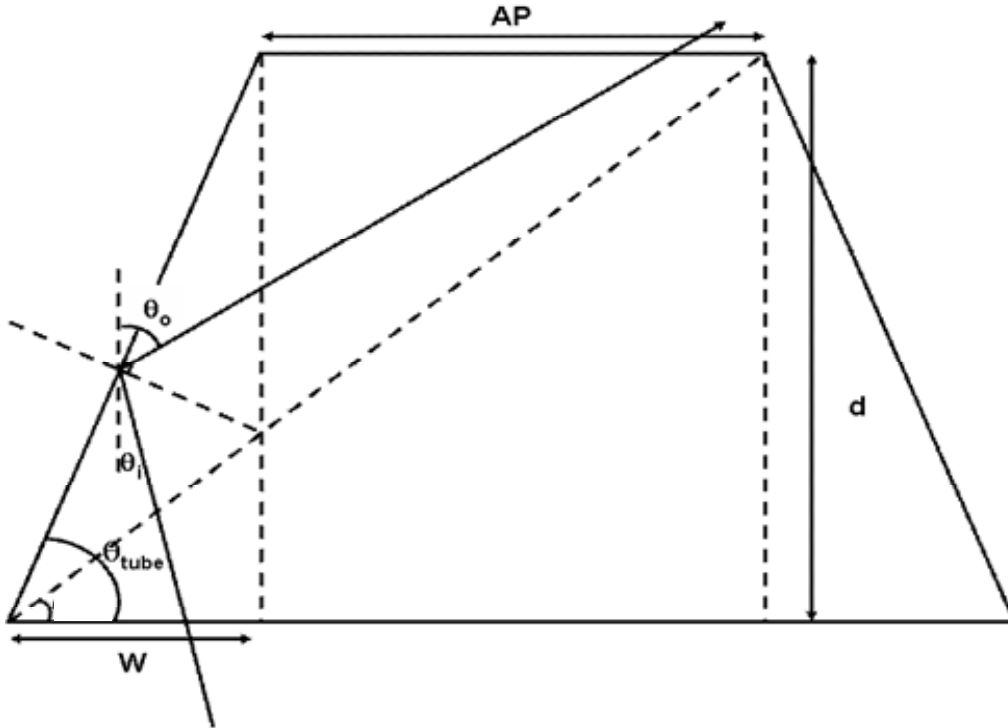


Fig. 4.2 Illustrative figure of the parameters for designing micro-tube structure.

The relevant equations are shown as follows. According to the trigonometric function, the following Eqs.(1), (2) and (3) can be given.

$$W = \frac{d}{\tan \theta_{tube}} \quad \text{Eq.(4.1)}$$

$$\tan \theta_1 = \frac{d}{AP + W} \quad \text{Eq.(4.2)}$$

$$\theta_1 = \tan^{-1}\left(\frac{d}{AP + W}\right) = \tan^{-1} = \tan^{-1}\left(\frac{d \cdot \tan \theta_{tube}}{AP \cdot \tan \theta_{tube} + d}\right) \quad \text{Eq.(4.3)}$$

Furthermore, in two right triangles, it is apparent that:

$$\begin{aligned}\theta_{tube} + \theta_3 &= 90^\circ \\ \theta_3 + \theta_i + \theta_2 &= 90^\circ\end{aligned}\quad \text{Eq.(4.4)}$$

Hence

$$\theta_2 = \theta_{tube} - \theta_i \quad \text{Eq.(4.5)}$$

According to reflective relationship,  $\theta_o$  can be given by

$$\theta_o = 180^\circ - \theta_i - 2 \cdot \theta_2 = 180^\circ - 2\theta_{tube} + \theta_i \quad \text{Eq.(4.6)}$$

Eq.(4.6) is tenable for each point on the tube. Hence

$$\theta_{oa(\max)} = 180^\circ - 2\theta_{tube} + \theta_{ia(\max)} \quad \text{Eq.(4.7)}$$

According to the definition of  $\theta_{oa(\max)}$  in Fig. 4.1.

$$\begin{aligned}\theta_{oa(\max)} &= 90^\circ - \theta_1 \\ \theta_{oa(\max)} &= 180^\circ - 2\theta_{tube} + \theta_{ia(\max)}\end{aligned}\quad \text{Eq.(4.8)}$$

Eq.(4.8) is to substitute  $\theta_1$ . Hence

$$\theta_{ia(\max)} = 2\theta_{tube} - 90^\circ - \tan^{-1}\left(\frac{d \cdot \tan \theta_{tube}}{AP \cdot \tan \theta_{tube} + d}\right), \quad \text{Eq.(4.9)}$$

where  $\theta_{ia(\max)}$  is defined as the MIA at point A as mentioned above and  $\theta_{oa(\max)}$  is the corresponding reflective angle.

Similar argument can be applied to other points on the tube wall and then there will be a  $\theta_{i(\max)}$  for every point of the tube wall. Because the MIA ( $\theta_{ia(\max)}$ ) at point A is the smallest among all points, as long as  $\theta_{ia(\max)}$  can be as large as possible and then more incident light can satisfy the constraint. Therefore, the tube can have better capability of collecting light.

As can be seen in Eq.(4.9),  $\theta_{ia(\max)}$  depends on  $\theta_{tube}$ , AP and d. As a result, the structure of micro-tube array has a significant influence on its capability of collecting light. In the following sections, the capability of the micro-tube for collecting light will

be further analyzed so that the optimized structure can be determined.

First, the light efficiency and light efficiency enhancement of the micro-tube array must be defined. These definitions are demonstrated by using the optical simulation software-ASAP. As shown in Fig. 4.3(a), considering the backlight source is projected onto the structure without micro-tube array, the ratio of light flux measured by the detector to the original total light flux is defined as X %. In addition, considering the same light source is projected onto the structure with micro-tube array, the ratio of light flux measured by the detector to the original total light flux is defined as Y %, as shown in Fig. 4.3(b). Herein, Y % is treated as light efficiency of micro-tube array and light efficiency enhancement is defined as Y % divided by X %.

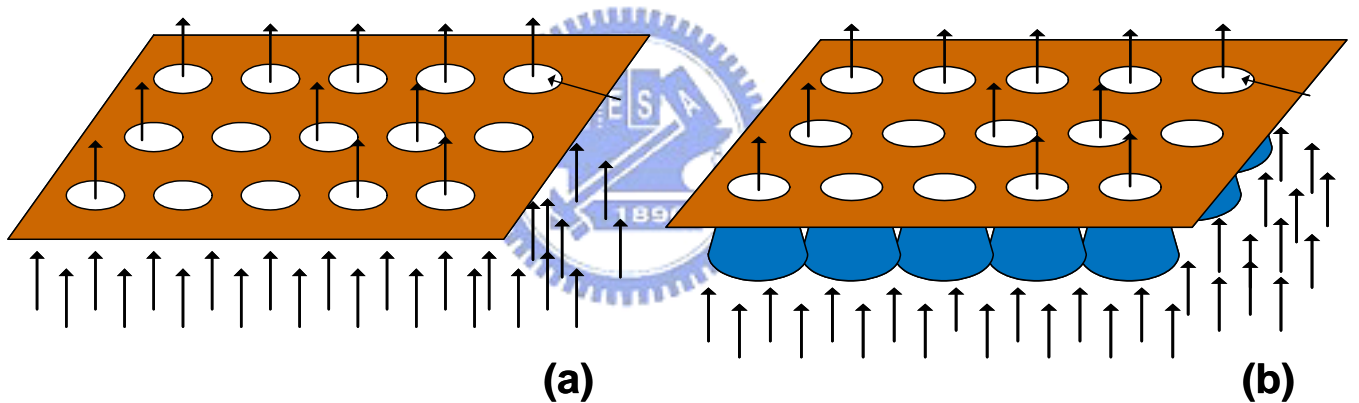


Fig. 4.3 Schematics for definitions of light efficiency and light efficiency enhancement.

A structure (a) without micro-tube array and (b) with micro-tube array

Considering only a single tube structure and the parallel light as backlight source, the ratio of light fluxes is equal to the area ratio, i.e. X % is equal to the ratio of the upper aperture to the total area and Y % is equal to the ratio of the lower aperture to the total area, where total area means the whole region of comprising a single tube. The values of X% and Y% can be given as follows.

$$X\% = \frac{\pi \cdot \left(\frac{AP}{2}\right)^2}{Total\ area} \quad \text{Eq.(4.10)}$$

$$Y\% = \frac{\pi \cdot \left(\frac{AP}{2} + W\right)^2}{Total\ area} \quad \text{Eq.(4.11)}$$

Therefore, light efficiency and light efficiency enhancement for a single tube structure can be calculated.

$$light\ efficiency = Y\% \quad \text{Eq.(4.12)}$$

$$light\ enhancement = \frac{Y\%}{X\%} = \left(1 + \frac{2W}{AP}\right)^2 \quad \text{Eq.(4.13)}$$

Eq.(4.1) is to substitute W. Hence

$$light\ efficiency\ enhancement = \left(1 + \frac{2d}{AP \cdot \tan \theta_{tube}}\right)^2 \quad \text{Eq.(4.14)}$$

From Eq.(4.14), it can be concluded that light efficiency depends on  $\theta_{tube}$ , AP and d. Therefore, the optimized design of micro-tube array requires the structure with the highest light efficiency enhancement. In the following analysis, ASAP was utilized to analyze the relationship between light efficiency enhancement and the structure on condition that parallel light was taken as the light source and projected to a single tube structure.

At first, AP was fixed as 5 $\mu$ m (Fig. 4.4),  $\theta_{tube}$  varied from 45° to 65° at 5° intervals, and then the relationship between the light enhancement and d was formed. It is apparent from this figure that the light efficiency enhancement decreased gradually as d decreased from 4 $\mu$ m to 2 $\mu$ m. As a result, a longer structure has better capability of collecting light.



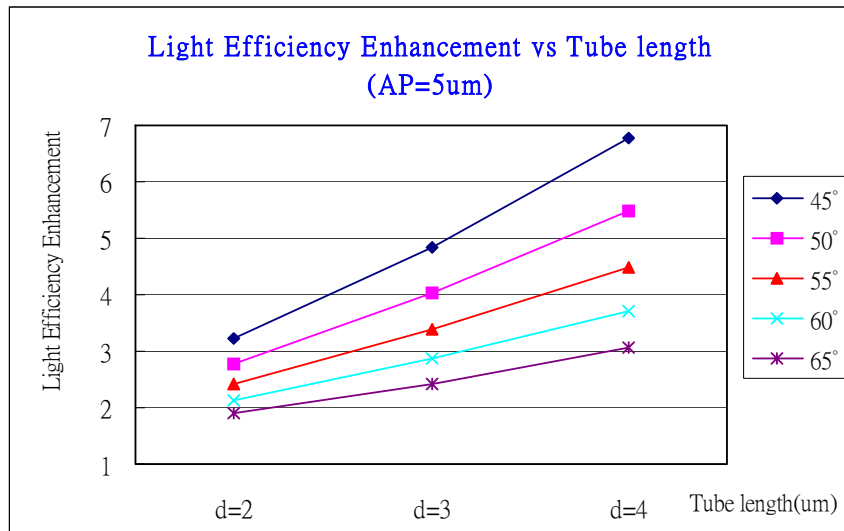


Fig. 4.4 Illustration of the relationship between light efficiency enhancement and d at AP=5

Moreover, d was fixed as 3um (Fig. 4.5),  $\theta_{\text{tube}}$  varied from 45° to 65° at 5° intervals, and then the relationship between the light efficiency enhancement and AP was plotted. It is observed that when AP increased from 4um to 6um, on the contrary, the light efficiency enhancement decreased gradually. Therefore, it can be concluded that a larger aperture can result in higher light efficiency, but not necessarily higher light efficiency enhancement.

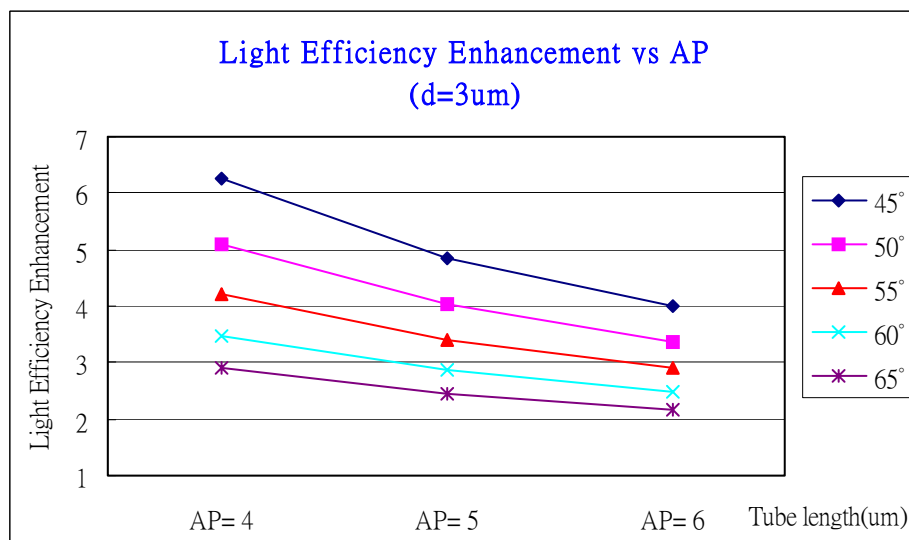


Fig. 4.5 Illustration of the relationship between light efficiency enhancement and AP at d=3um

### 4.3.2 Simulation Results of BEF and BEF and Optimization

In the previous analysis, we considered that parallel light was taken as a backlight source. However, most of the backlight sources utilized in commercial transfective LCDs make use of Brightness Enhancement Film-BEF II or BEF III [22] [23] to control the exit angles of the backlight. For the backlight sources (BEF II or BEF III), most of the light flux is distributed within the range from  $+20^\circ$  to  $-20^\circ$ . Fig. 4.6 illustrates the light flux distributions of BEF II and BEF III, respectively, simulated by ASAP.

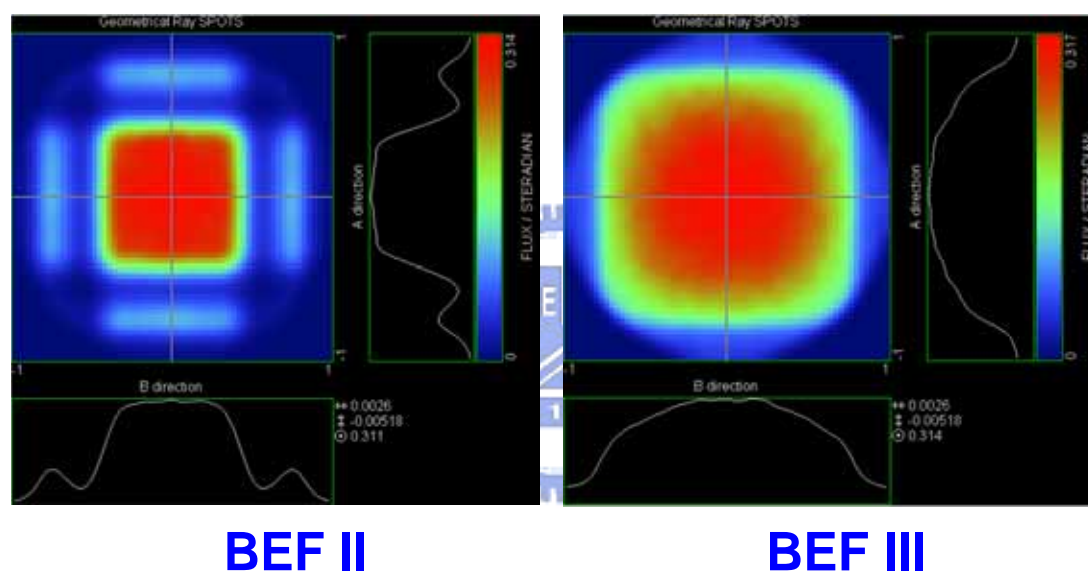


Fig. 4.6 Light flux distributions of backlight sources with the addition of optical films-BEF II and BEF III.

In the following analysis, we further broadened the analysis by considering a micro-tube array on a sub-pixel and BEF II and BEF III were taken as the light sources in order to verify the capability of this design for collecting light.

First, the parameter setting is shown in Fig. 4.7, where AP is the diameter of upper aperture, d is the depth (length) of the micro-tube and  $\theta_{\text{tube}}$  is the tilt angle of the tube. Fig 4.7(b) shows a top view of a micro-tube array simply, in which R is defined as the radius of lower aperture and width is defined as a periodic width of the lower aperture

in this array. Assuming the distance between adjacent lower apertures is 0.2um, and then R and width can be derived as follows.

$$R = \frac{d}{\tan \theta_{tube}} + \frac{AP}{2} \quad \text{Eq.(4.15)}$$

$$width = 2 \cdot R + 0.2 \quad \text{Eq.(4.16)}$$

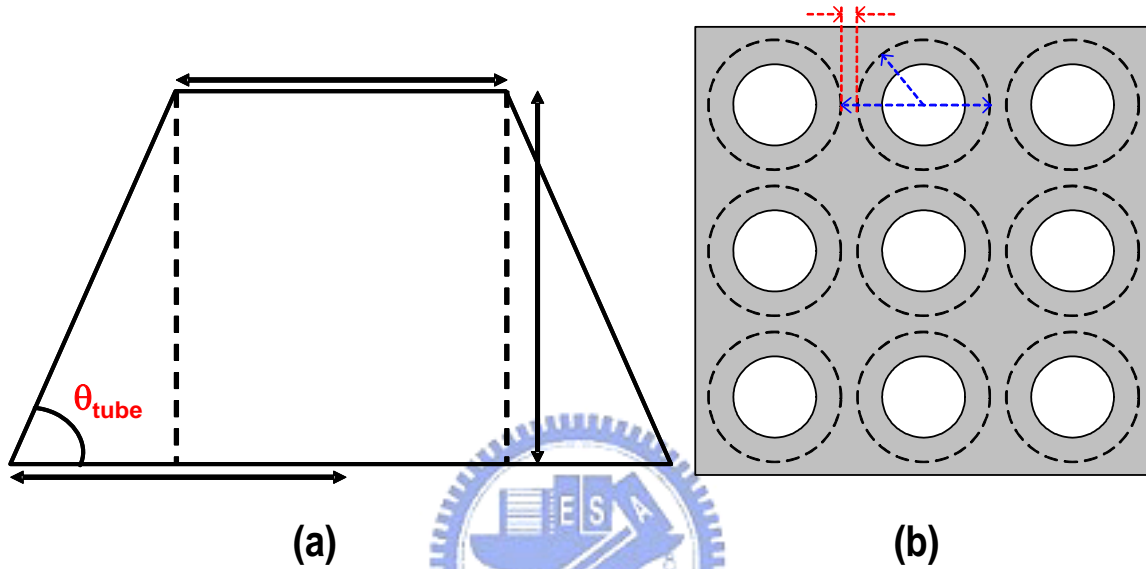


Fig. 4.7 The parameter setting for a micro-tube array. (a) A lateral view of a single tube structure. (b) A top view of a micro-tube array.

Herein, the micro-tube array was built on a sub-pixel of which the area is 70um x 210um. Because the space between adjacent sub-pixels is about 6um, the available area is only 64um x 204um. When the distribution of the micro-tube array was determined, the optical simulation software ASAP was utilized to analyze the light efficiency and light efficiency enhancement for parallel backlight.

We had concluded from Figs. 4.4 and 4.5 that a longer tube has higher collecting efficiency and a smaller aperture can result in higher light efficiency enhancement. But, due to the limitation in the fabrication process, the specification of the structures with  $d=3\mu\text{m}$  and  $AP=4$  or  $5\mu\text{m}$  was chosen to make a further analysis. The results are shown

in Figs. 4.8 and 4.9, which represent the relative curves of AP to light efficiency and light efficiency enhancement on condition that the  $d$  is fixed at  $3\mu\text{m}$  and the  $\theta_{\text{tube}}$  varies from  $45^\circ$  to  $80^\circ$  for BEF II and BEF III, in which the AP equals to  $5\mu\text{m}$  in Fig. 4.8 and  $4\mu\text{m}$  in Fig. 4.9. As observed, there is a similar tendency between BEF II and BEF III light sources. Besides, the tendency of the light efficiency as a function of  $\theta_{\text{tube}}$  is nearly linear, therefore the structure with larger  $\theta_{\text{tube}}$  has higher light efficiency. Besides, light efficiency enhancement increases to the peak at an angle of  $60^\circ$  and then drop when beyond  $60^\circ$ . Although the light efficiency increases linearly with the increase of  $\theta_{\text{tube}}$ , the light efficiency enhancement decreases at large  $\theta_{\text{tube}}$ . This is a trade-off, therefore the desired result is that the light efficiency is greater than 50% and light efficiency enhancement is greater than a factor of 1.5. Under this condition the useful structure of micro-tube array was determined. In the end, we chose the micro-tube array with the specifications of  $d=3\mu\text{m}$ ,  $\theta_{\text{tube}}=60^\circ$  and  $\text{AP}=5\mu\text{m}$  for the applications.

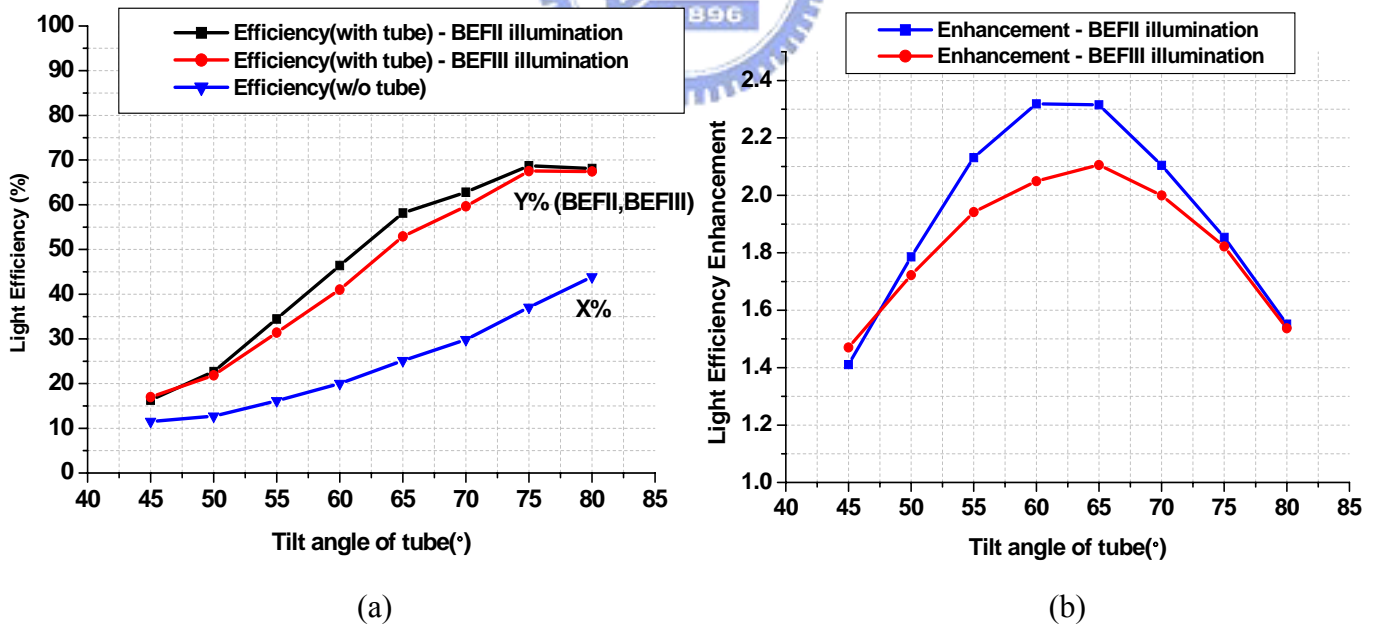


Fig. 4.8 The relative curves of  $\theta_{\text{tube}}$  versus (a) light efficiency and (b) light efficiency enhancement on condition that  $d$  is fixed at  $3\mu\text{m}$  and AP is fixed at  $5\mu\text{m}$ .

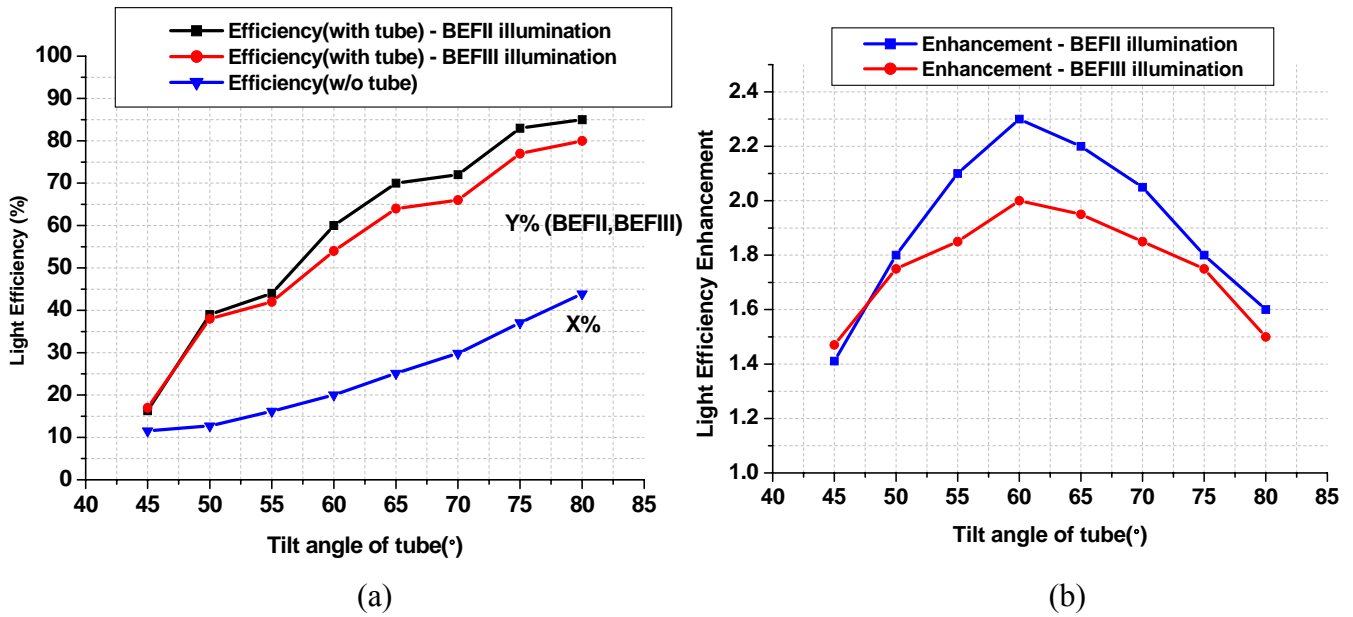
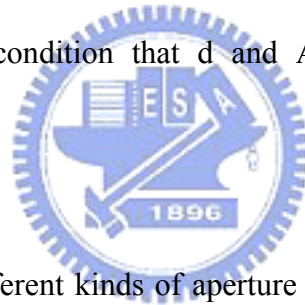


Fig. 4.9 The relative curves of  $\theta_{\text{tube}}$  versus (a) light efficiency and (b) light efficiency enhancement on condition that  $d$  and  $AP$  are fixed at  $3\mu\text{m}$  and  $4\mu\text{m}$ , respectively.



#### 4.4 Simulation of Structure

In this section, three different kinds of aperture shapes were used to simulate the properties of light utilization efficiency and light distribution so that further analyses were made to decide other parameters of the optimized structure.

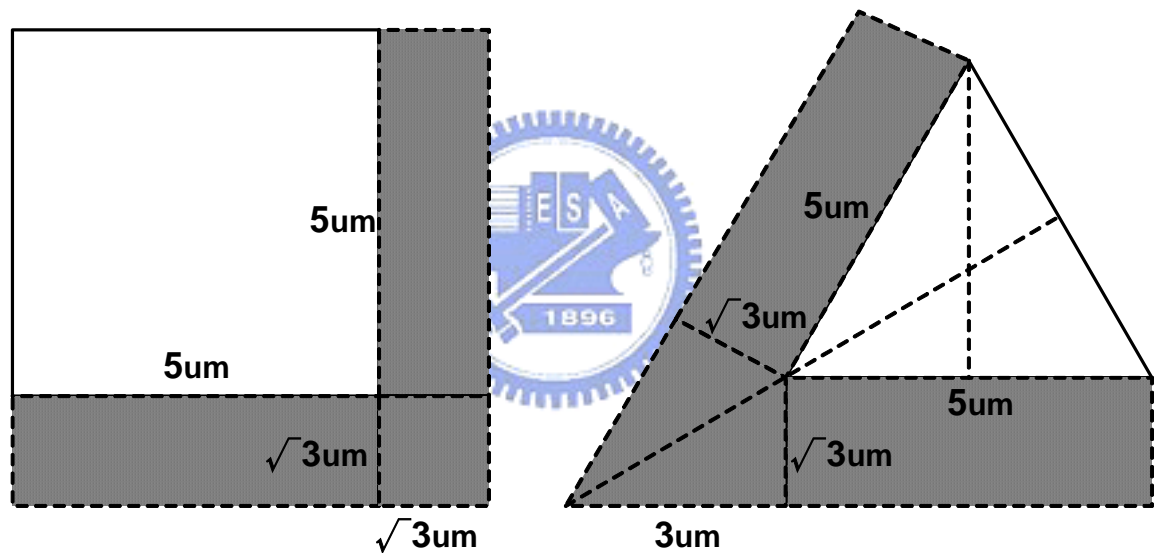
##### 4.4.1 Comparison between Different Aperture Shapes

Due to process limitation, the minimum line width between the critical dimensions should be larger than  $5\mu\text{m}$ . Therefore, the above rule must be followed in the analysis for the structures presented below. In particular, a structure with triangular aperture had been included in the analysis. The reasons why this shape was chosen are as follows.

The area of the upper aperture is smaller in a triangle than in a square when each side equals to  $5\mu\text{m}$  is taken into consideration. Namely, the area allowing the backlight for direct transmission is smaller. Therefore, more triangular upper apertures can be

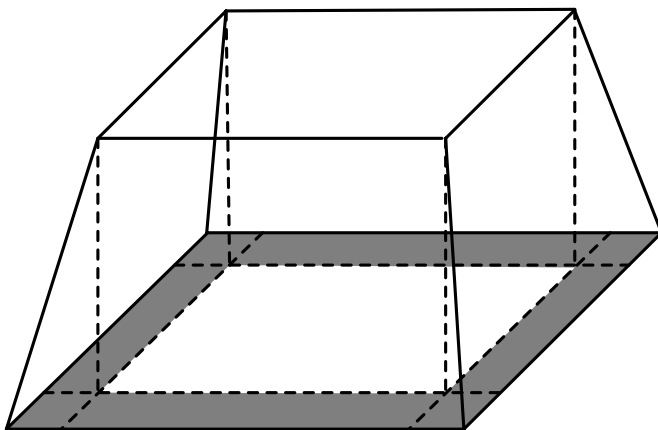
arranged on one sub-pixel than square aperture.

A triangle can provide larger area for light efficiency enhancement. The term “the area for light efficiency enhancement” was defined as the lower aperture area minus the upper aperture area. It corresponded to the vertical projection area of the tube-wall. The shaded areas in Fig. 4.10 depict the area for light efficiency enhancement. In a triangular micro-tube structure, the ratio of a lower-aperture area to an upper-aperture area is larger than a square micro-tube structure because of the area for light efficiency enhancement. Therefore, the triangular micro-tube structure should have a higher light efficiency enhancement.

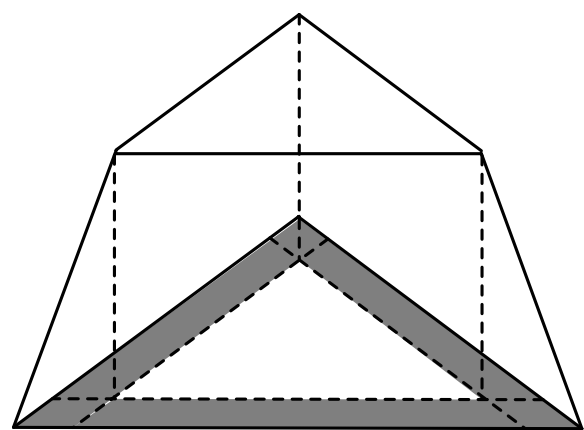


(a) 2-D picture of a square aperture

(b) 2-D picture of a triangular aperture



(c) 3-D picture of a square aperture



(d) 3-D picture of a triangular aperture

Fig. 4.10 Schematics of “the area for light efficiency enhancement” for comparison between a square and a triangle.

The following simple calculation **validated** this conclusion according to the data in **Figs. 4.10(a) and (b)**.

In a square micro-tube structure:

$$A \text{ upper-aperture area} = 5 \times 5 = 25 \quad (\mu\text{m}^2) \quad \text{Eq.(4.17)}$$

$$\text{The shaded area} = \sqrt{3} \times \sqrt{3} \times 4 + 5 \times \sqrt{3} \times 4 = 46.64 \quad (\mu\text{m}^2) \quad \text{Eq.(4.18)}$$

$$A \text{ lower-aperture area} = 25 + 46.64 = 71.64 \quad (\mu\text{m}^2) \quad \text{Eq.(4.19)}$$

#### The area ratio for light efficiency enhancement

$$= \frac{A \text{ lower-aperture area}}{A \text{ upper-aperture area}} = 2.87 \quad \text{Eq.(4.20)}$$

In a triangular micro-tube structure

$$A \text{ upper-aperture area} = 5 \times \frac{5\sqrt{3}}{2} \times \frac{1}{2} = 10.83 \quad (\mu\text{m}^2) \quad \text{Eq.(4.21)}$$

$$\text{The shaded area} = 3 \times \sqrt{3} \times 3 + 5 \times \sqrt{3} \times 3 = 41.56 \quad (\mu\text{m}^2) \quad \text{Eq.(4.22)}$$

$$A \text{ lower-aperture area} = 10.83 + 42.56 = 52.39 \quad (\mu\text{m}^2) \quad \text{Eq.(4.23)}$$

#### The area ratio for light efficiency enhancement

$$= \frac{A \text{ lower-aperture area}}{A \text{ upper-aperture area}} = 4.84, \quad \text{Eq.(4.24)}$$

where the area ratio of a lower-aperture to an upper-aperture **corresponded** to the light efficiency enhancement.

#### 4.4.2 Simulation Results for Different Aperture Shapes

The three kinds of shapes, **as presented in Fig. 4.11**, **were** analyzed by ASAP and compared. The BEFII, BEFIII **were** taken as the light sources, the number of rays **was**

set to 480000, the tilt angle was  $60^\circ$  and the tube length was  $3\mu\text{m}$ . Figs. 4.12 and 4.13 show the simulation results according to the above conditions. From the figures, it is observed that the square aperture has the maximum light efficiency because of its largest aperture area. Besides, the light efficiency for the triangular aperture is less than 20%, and this value is low in comparison with other shapes. Furthermore, all of the three shapes have high light efficiency enhancement more than by a factor of 1.5, and this corresponds to our demands for the transmissive light.

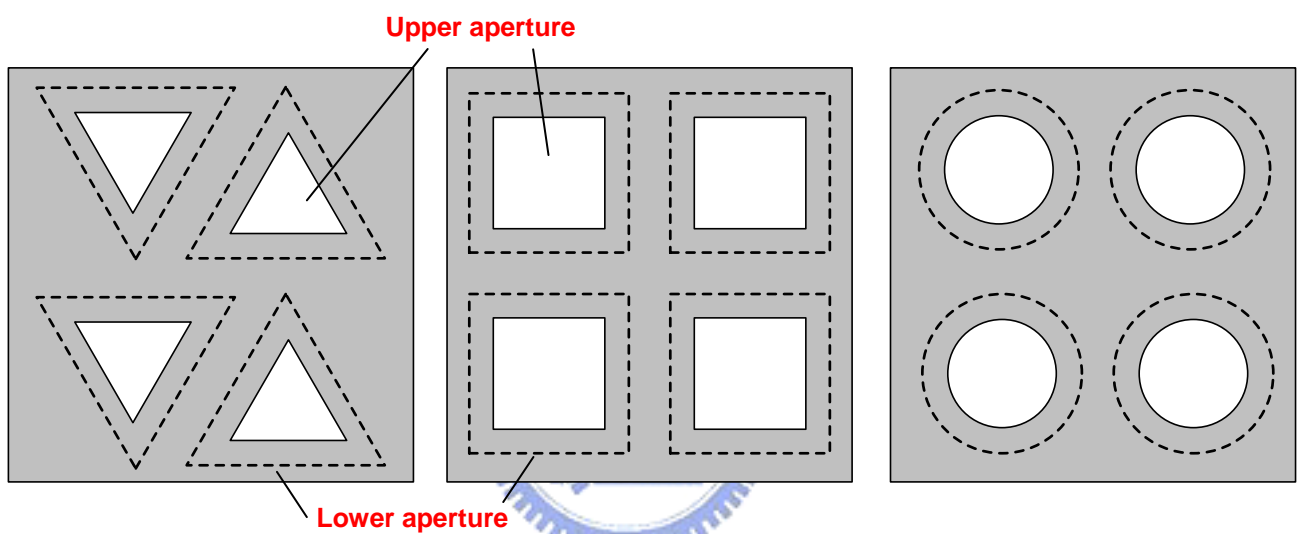


Fig. 4.11 Illustration of the structure for three kinds of aperture shapes

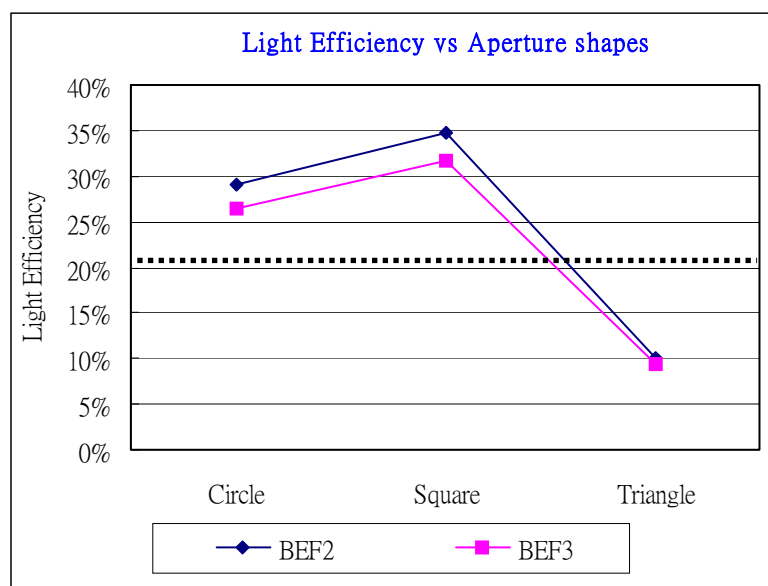


Fig. 4.12 Relationship between light efficiency and shapes for BEF II and BEF III.



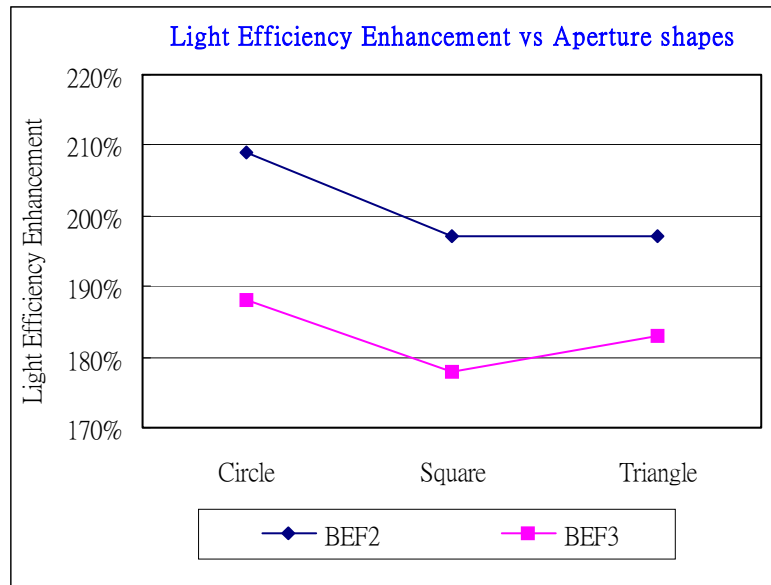
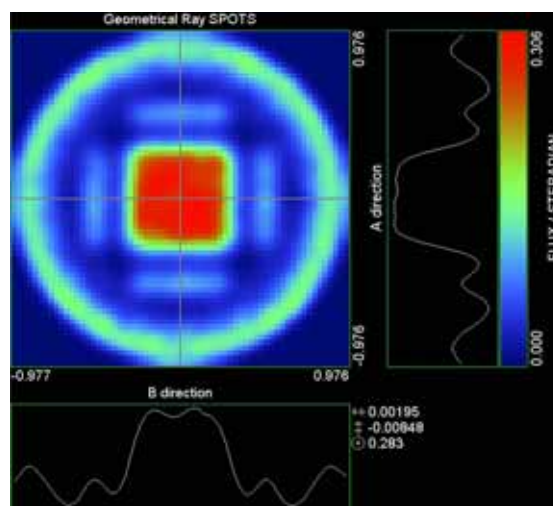
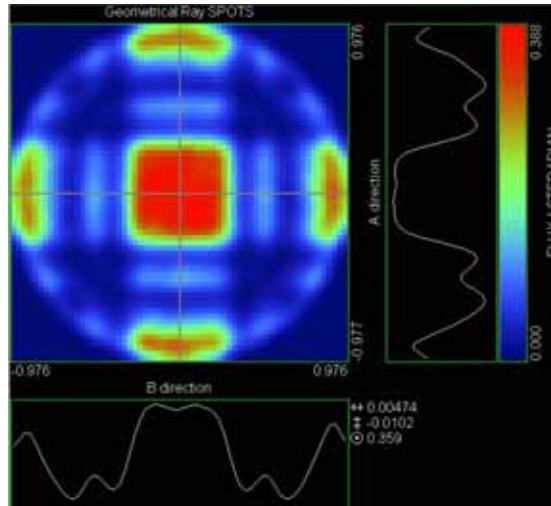


Fig. 4.13 Relationship between light efficiency enhancement and shapes for BEF II and BEF III.

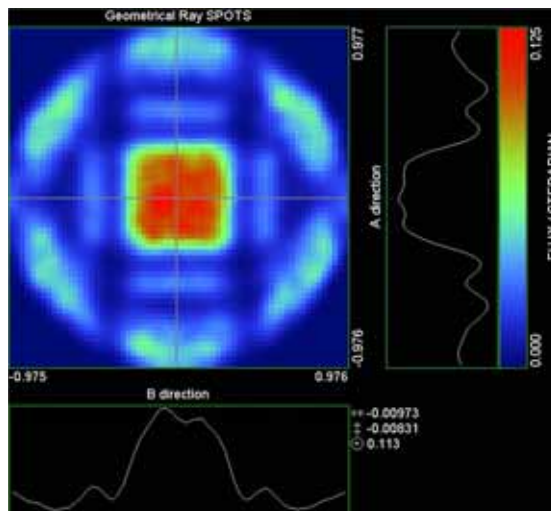
Luminance flux distributions (BEFII) of the above three types were demonstrated by ASAP, as shown in Fig. 4.14. It is observed that the luminance flux for the circular structure presents a uniform ring-like distribution. For the square structure, the flux is distributed principally in four directions. Besides, the luminance flux distribution is a hexagon for the triangular structure.



(a) Micro-tube array with circular upper apertures



(b) Micro-tube array with rectangular upper apertures



(c) Micro-tube array with triangular upper apertures

Fig. 4.14 Simulated luminance flux distribution diagram for BEFII light source by ASAP.

Micro-tube array with (a) circular upper apertures, (b) rectangular upper apertures, and (c) triangular upper apertures

According to the simulated results from Figs. 4.12, 4.13 and 4.14, several conclusions can be made as below.

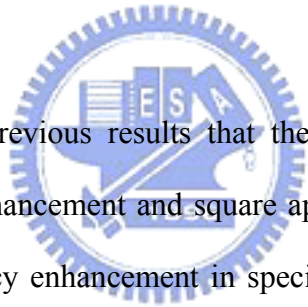
(a) Square shape **has** the best light efficiency, then circular and triangular ones in turn.

(b) Although the circular aperture **possesses** the maximum overall light efficiency enhancement, its intensity in each direction **is** a reduced ring-like distribution of

backlight as shown in Fig 4.14.

- (c) Compared with the circular aperture, the overall light efficiency enhancement is smaller for a square aperture. However, it has larger brightness enhancement in the specific directions due to its flux distribution in only four directions.
- (d) The light efficiency enhancement is not very high for a triangular structure and this is significantly different from our previous expectation. We further analyzed this issue by using optical software, and found “the area for light efficiency enhancement” in the triangular structure causes the incident backlight encounters multi-reflection, and a half of rays exits from the lower aperture. As a result, the light cannot be efficiently utilized.

#### 4.5 Mask Design



It is known from the previous results that the circular aperture possesses the maximum light efficiency enhancement and square aperture is in the next place. Only considering the light efficiency enhancement in specific directions, square aperture is more ideal. As to the triangular aperture, it does not have preferable light efficiency enhancement as expected. Therefore, only circular and square apertures were considered in subsequent mask design, and furthermore the aperture shapes for regular and irregular arrangements were also considered in the design, respectively.

##### 4.5.1 Regular Pattern

First, the regularly-arranged shapes were considered. Because the minimum line width must be equal to  $5\mu\text{m}$ , we took several conditions into considerations as shown in Tables 4.1 and 4.2. In table 4.1, the specification was chosen, in which the length of the upper aperture is  $5\mu\text{m}$  and the distance between the adjacent upper apertures is  $7\mu\text{m}$ . This is because we considered that the tube length is  $5\mu\text{m}$  and the tilt angle is  $60^\circ$ , and

then the lower aperture is 2 $\mu$ m slightly larger than the upper aperture. The mask must be designed as described above in order to meet the limitation of minimum line-width.

Table 4.1 The list of the specifications for regularly-arranged square aperture.

Square aperture		
the length of upper aperture ( $\mu$ m)	the distance between adjacent upper apertures ( $\mu$ m)	notation
5	7	(squ. L5_D7)
5	11	(squ. L5_D11)
7	7	(squ. L7_D7)
7	11	(squ. L7_D11)

Table 4.2 The list of the specifications for regularly-arranged circular aperture.

Circular aperture		
the length of upper aperture ( $\mu$ m)	the distance between adjacent upper apertures ( $\mu$ m)	notation
5	7	(squ. L5_D7)
5	11	(squ. L5_D11)
7	7	(squ. L7_D7)
7	11	(squ. L7_D11)

After the specifications were determined, ASAP was utilized to further analyze these structures with different sizes and shapes. As shown in Table 4.3, the light efficiency and light efficiency enhancement was calculated on condition that BEFII and BEFIII were taken as light sources. From the tables, it is apparent that light efficiency enhancement is still fairly high, but light efficiency has gone down substantially because of larger space between the adjacent apertures.

Table 4.3 Light efficiency and enhancement calculated for various sizes and shapes

(a) Micro-tube array with circular upper apertures

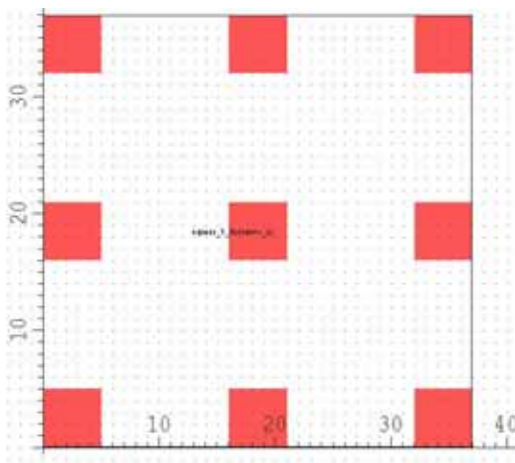
		BEF II		BEF III	
L	D	Efficiency	Enhancement	Efficiency	Enhancement
5	7	29.17%	× 2.09	26.36%	× 1.88
5	11	16.48%	× 2.04	14.84%	× 1.84
7	7	32.80%	× 1.82	30.47%	× 1.67
7	11	19.46%	× 1.83	18.07%	× 1.68

(b) Micro-tube array with square upper apertures

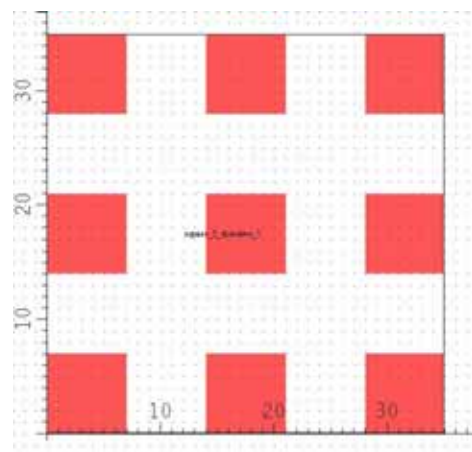
		BEF II		BEF III	
L	D	Efficiency	Enhancement	Efficiency	Enhancement
5	7	34.85%	× 1.97	31.61%	× 1.78
5	11	19.65%	× 1.93	17.77%	× 1.74
7	7	39.73%	× 1.74	36.74%	× 1.59
7	11	23.49%	× 1.74	21.75%	× 1.59

Furthermore, according to the above specifications we made use of the software-L-edit to draw the regularly-arranged aperture shapes in the mask, as shown in

Fig. 4.15.



(a) (squ.\_L5\_D11)



(b) (squ.\_L7\_D7)

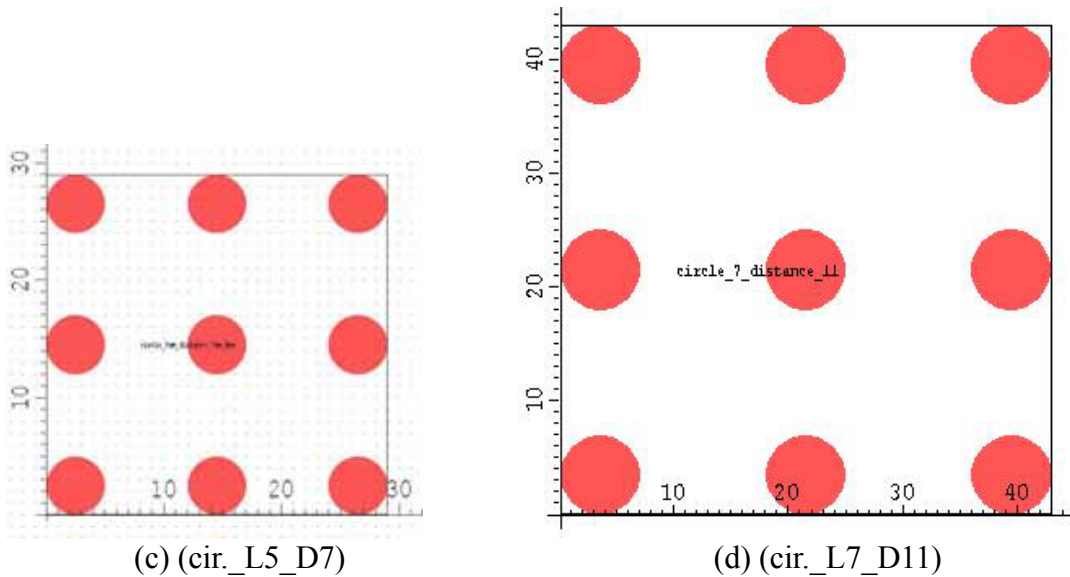
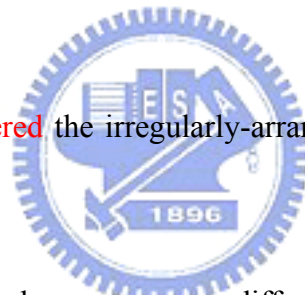


Fig. 4.15 Regular shapes drawn by L-edit

(a) (squ\_L5\_D11) (b) (squ\_L7\_D7) (c) (cir\_L5\_D7) (d) (cir\_L7\_D11)

#### 4.5.2 Irregular Pattern

Furthermore, we considered the irregularly-arranged shapes. The design is based on the considerations below.



- (a) It can avoid the moiré phenomenon or diffraction effects caused by regular arrangement so that the light efficiency or other image qualities can be further improved.
- (b) According to users' demands, for example, considering higher brightness of the reflective region, the square and rectangular apertures can be arranged randomly according to different ratios in number and various sizes. Besides, the square and rectangular shapes can be also replaced by circular or elliptical shapes.

Then, we made use of the software-L-edit to draw the irregularly-arranged apertures in the mask, as shown in Fig. 4.16.

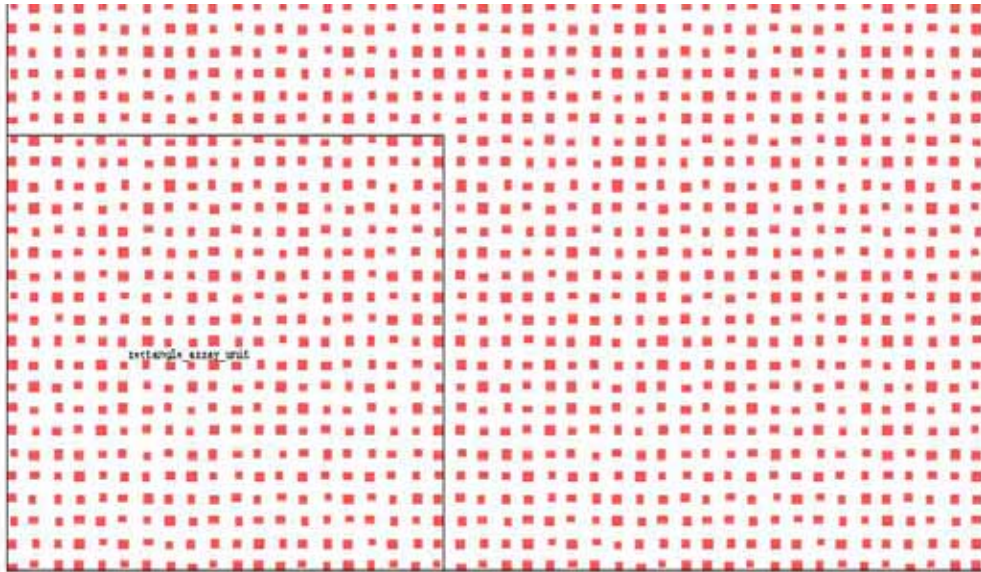


Fig. 4.16 Schematic figure of mask prototypes comprising irregularly-arranged apertures

Finally, a mask comprising various sizes and shapes of the apertures in regular and irregular arrangements can be achieved as follows.

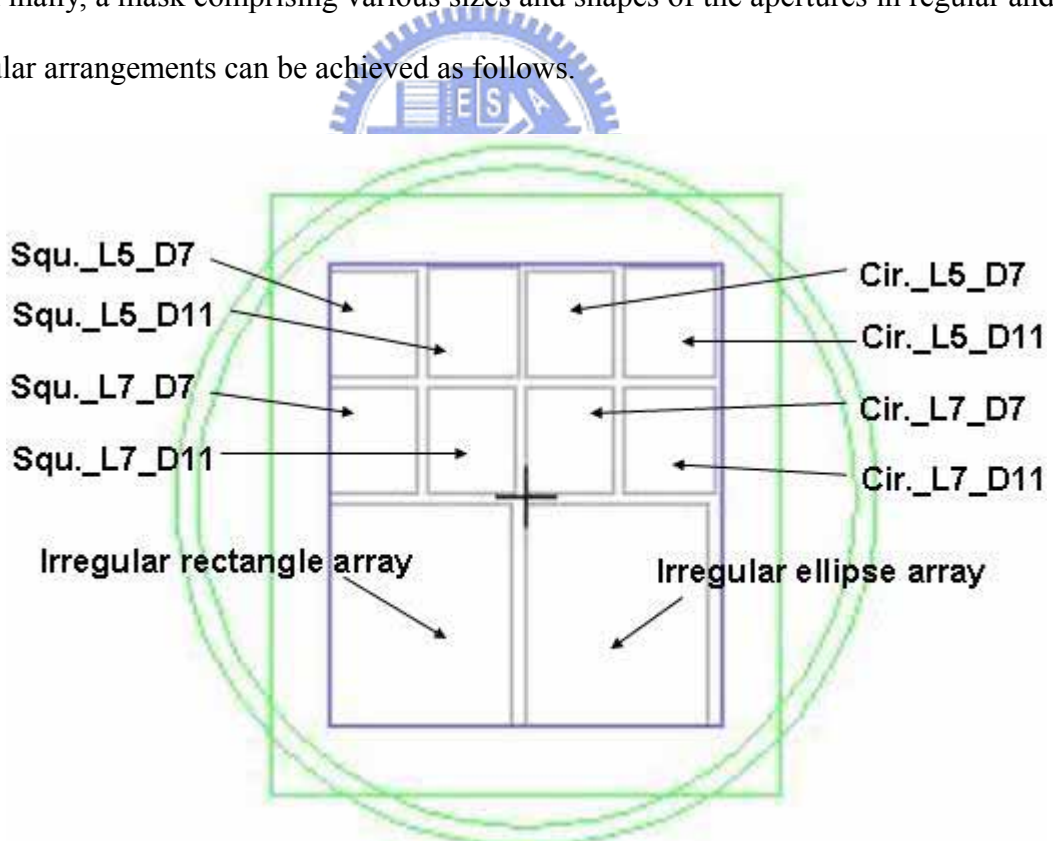
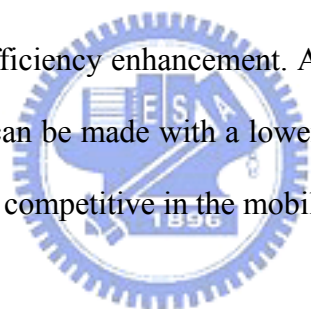


Fig. 4.17 Schematic diagram of the mask comprising various aperture shapes in regular and irregular arrangements

#### 4.6 Summary

We have designed and optimized the micro-tube array structure. It **is** recognized from the mentioned analyses that the structure of micro-tube array **has** the distinguished capability for the collection of light; therefore light efficiency and light efficiency enhancement of backlight sources can be increased significantly. Additionally, for the conventional transfective LCDs, the main light source **is** the reflective ambient light and the backlight system only **serves** an auxiliary role. As a result, after the light efficiency enhancement **is** increased effectively by the micro-tube array, area ratio of the reflective region to the transmissive region can be redistributed so that the brightness of the reflective light can be further enhanced. On the other hand, the backlight system can be utilized to achieve the same illumination as conventional transfective LCDs by light efficiency enhancement. As a result, the novel transfective LCDs with micro-tube array can be made with a lower power consumption or decrease in weight, which will be more competitive in the mobile display applications.





# Chapter 5

## Experimental Results and Discussion

### 5.1 Introduction

According to the previous fabrication process with conventional fabrication recipes, in which the exposure time was 20sec for the 1<sup>st</sup> mask and 1.46sec for the 2<sup>nd</sup> mask, the 1<sup>st</sup> sample can be obtained. AFM was utilized to measure the fabricated structure, as shown in Fig. 5.1. It is apparent that the tube depth was only 0.48um which is slightly higher than the Al layer. Besides, the size of upper aperture was too small. Since the mask with an aperture size of 5um was utilized in exposure, the fabricated upper aperture was only 2.7um. Therefore, Al layer could not cover over the tube sidewall, which was attributed to a small upper aperture. This phenomenon was explained by the fact that the aperture of Al layer was determined by the exposure energy of the 2<sup>nd</sup> mask. Under the present situation, however, the opened aperture of Al layer was 5um, but, the upper aperture was only 2.7um in width. Therefore, some Al layer covering the tube sidewall would be removed by using an Aluminum acid. Compared with the simulation structure, this one was unavailable. A 3D picture from AFM demonstrates the said phenomenon more clearly, as shown in Fig. 5.2.

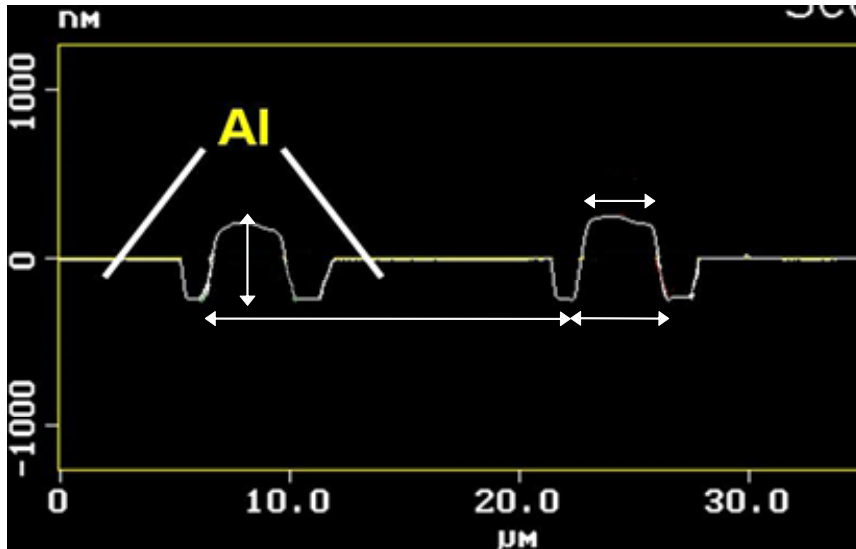


Fig. 5.1 Cross-section view of the fabricated structure from AFM.

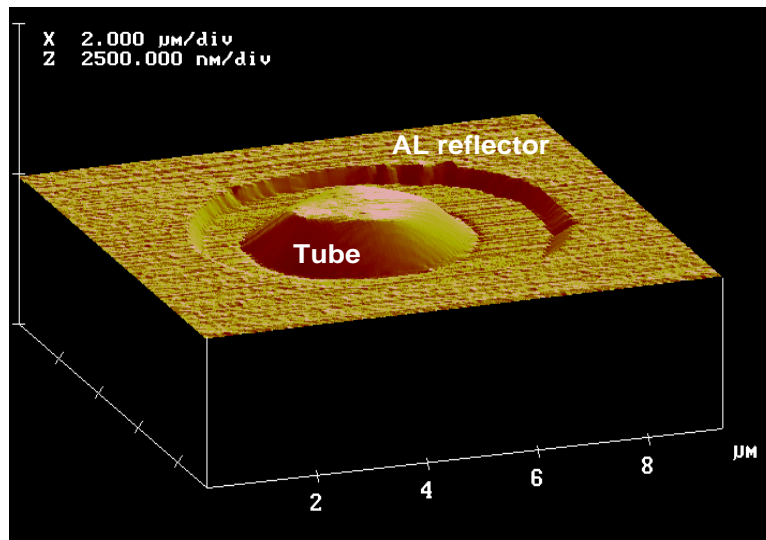


Fig. 5.2 A 3D picture of the fabricated structure from AFM

## 5.2 Diffraction Effect

The mentioned experimental results **can** be further interpreted well by the diffraction effect [24] [25]. Due to the diffraction effect, it **might** result in the superimposition of light energy. As shown in Fig. 5.3(a), when the distance between two rays of light **is** far, the diffraction effect **is** not obvious so that respective luminance flux distributions **are** complete and independent. However, when the distance **is** close enough to take the diffraction effect into consideration, it **will** cause the superimposition of light energy in the superimposed region. Therefore, for the exposure

of the 1<sup>st</sup> mask there **is** a superimposition of light energy under the sheltered region of the mask so that this region **will** suffer from more serious exposure.

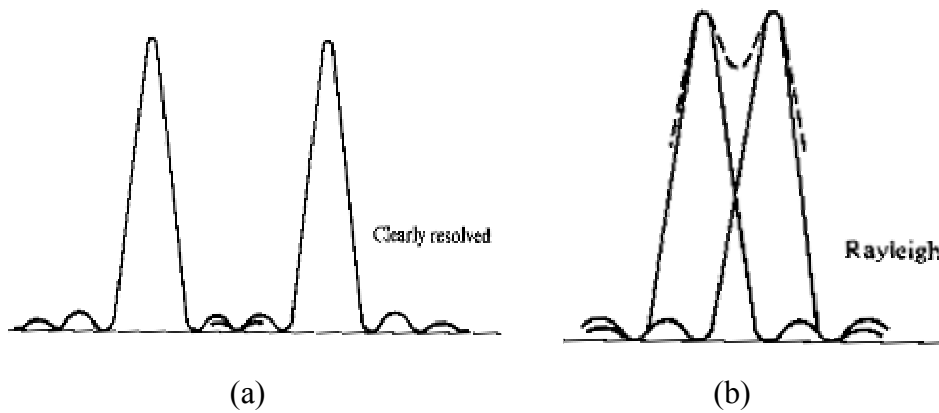


Fig. 5.3 Schematic explanation of the phenomenon (a) without and (b) with diffraction effect.

A further explanations with a diagrams shown in Fig. 5.4 are given as follows.

- (1) The exposure of the 1<sup>st</sup> mask **was** implemented to a 5 $\mu$ m thickness of organic layer.
- (2) The distribution of light energy **was** shown in Fig. 5.4(step 2) due to the diffraction effect. It **should** be noted that there **was** a slight exposure under the sheltered region of the mask based on the superimposition of light energy.
- (3) When **kept** on the exposure, the organic layer under the sheltered region **would** come off slightly all the time.
- (4) The phenomenon **would** be more and more serious so that a structure with short tubes and narrow upper apertures were **obtained**.
- (5) Then, an Al film **was** sputtered on the surface of the micro-tube array by a sputter coater. The Al-sputtered structure **was** spun coating with a positive photoresist.
- (6) The exposure of the 2<sup>nd</sup> mask **was** implemented. If the size of upper aperture

had been equal to the 2<sup>nd</sup> mask aperture as expected, there would only have been the photoresist above the upper aperture released. In fact, the upper aperture was too small so that the photoresist on the sidewall was released.

(7) When an Aluminum acid was utilized, all of the aluminum layer not covered with the photoresist would be removed. Therefore, the Al layer on the sidewall was also released.

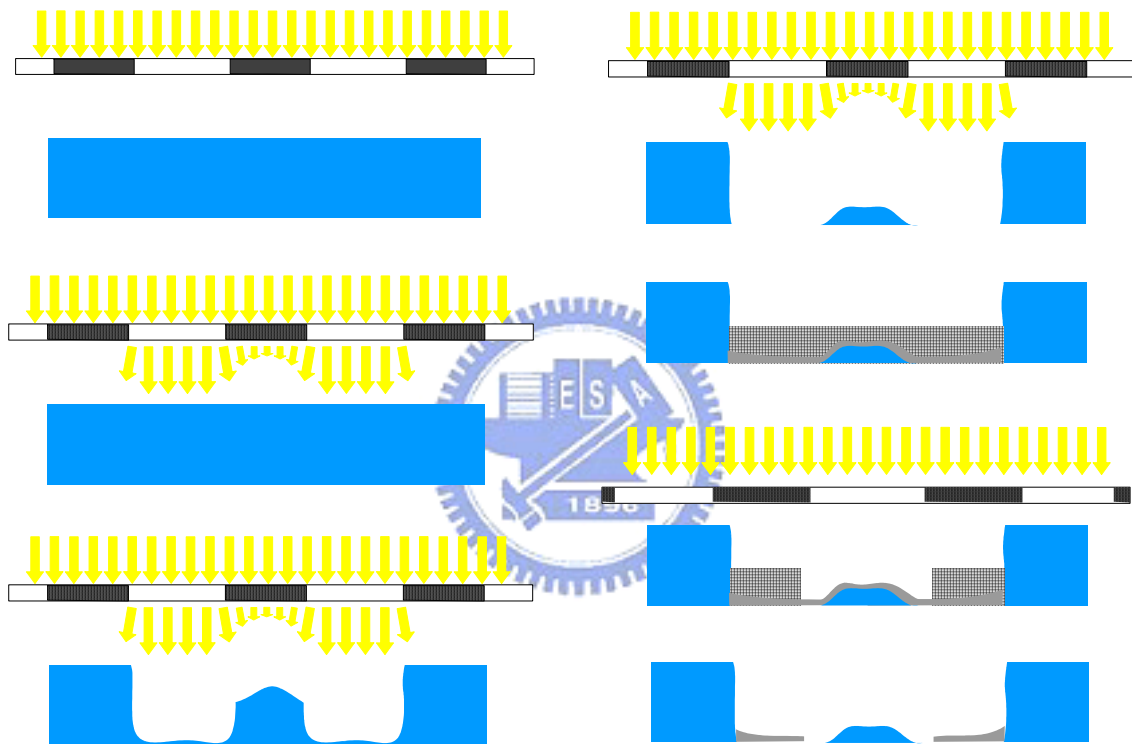


Fig. 5.4 Schematic explanation of diffraction effect in fabrication

Considering the priority of fabrication processes, we thought that there are four key parameters determining the partial structures of a single micro-tube respectively. Therefore, in order to solve the mentioned problem we proposed four methods to improve the structure. About these issues, a detail explanation will be given in the following sections.

### 5.3 Tube Depth

Considering the tube depth, the exposure time of the 1<sup>st</sup> mask played a leading role. Therefore, in order to reduce the problem caused by diffraction effect, the exposure time had to be shortened.

By shortening the exposure time, the influence of diffraction effect on the structure could be decreased effectively. However, it was worth noticing that the exposure time would have an optimized value. If the exposure time was less than the optimized value, the unnecessary organic layer around the tubes could not be released completely. Therefore, the tube would be too short.

On the premise that the size of mask aperture was fixed, the relationship between the height of tube and exposure time was shown in Fig. 5.5. Initially tube height would increase with the increase of exposure time. The line climbed up to the peak at 7sec, and then dropped significantly to the valley beyond 7sec. This curve was in agreement with the proposed hypothesis, that is to say, the diffraction effect led to the reduced micro-tube.

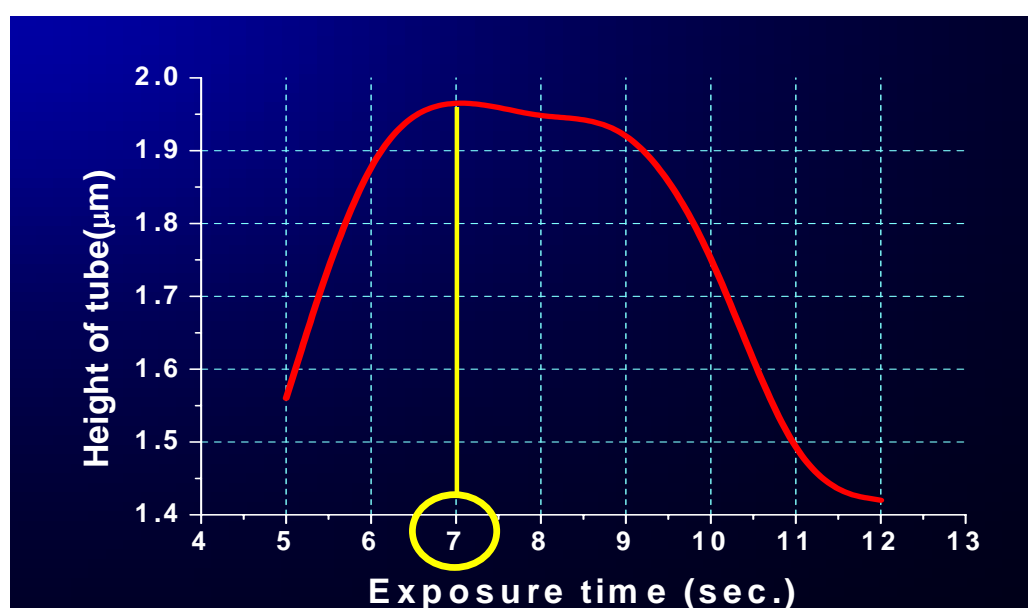


Fig. 5.5 Relationship between the height of tube and exposure time

The experimental result was demonstrated in Fig. 5.6, in which the exposure time was set as 7sec. It was seen in this figure that the improvement of micro-tube in height was very pronounced and it increased from 0.48um to 2.0um with the decrease of exposure time from 20sec to 7 sec. Besides, the Al layer covered slightly over the tube sidewall due to the heightened micro-tube. This phenomenon can be interpreted well by the fact that the heightened micro-tube resulted in a enlarged lower aperture. Therefore, considering the exposure of the 2<sup>nd</sup> mask, the tube sidewall can be covered with some photoresist so that the Al under the photoresist can be protected from being released by the Aluminum acid.

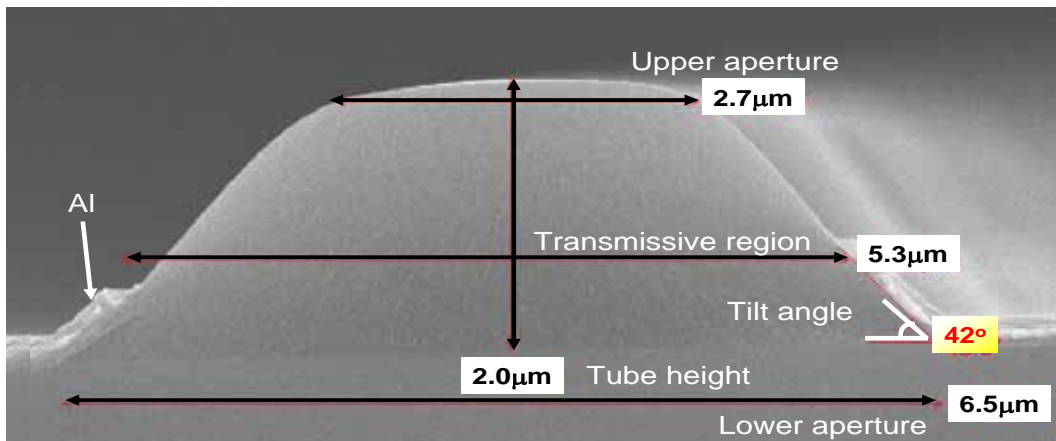


Fig. 5.6 A photograph of fabricated structure from SEM after exposure time was reduced

The same result can be observed in Fig. 5.7. It is a 3D AFM scan. The scale of the coordinate in Figs 5.2 and 5.7 was the same so that a comparison of these two figures was obviously in good agreement with the mentioned discussion.

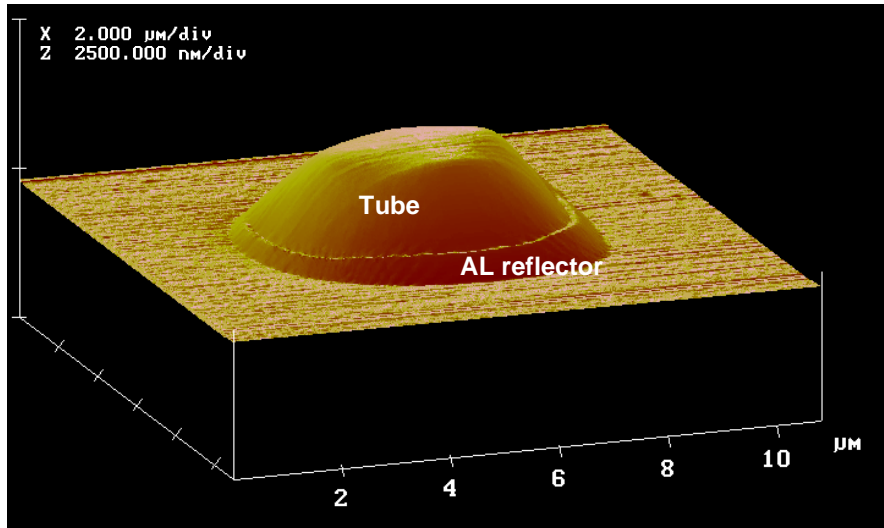


Fig. 5.7 A 3D AFM scan of the fabricated structure

#### 5.4 Upper Aperture

The second issue **was** relative to the size of mask aperture. Besides the exposure time of the 1<sup>st</sup> mask, the influence of diffraction effect on the structure can also be decreased by using different aperture sizes for the two masks. Furthermore, the problem about small upper aperture can also be solved at the same time. After analyzing the measured data from AFM, we **proposed** a novel mask specification. The aperture size of the 1<sup>st</sup> mask can be enlarged to cooperate with the original 2<sup>nd</sup> mask because a larger mask aperture can result in slighter diffraction effect and enlarge upper aperture of the tube.

According to the previous analyses, the fabricated upper aperture **was** about 2.5μm by the exposure of the 1<sup>st</sup> mask with a size of 5μm. Therefore, we utilized different aperture size, from 5μm to 8μm, of 1<sup>st</sup> mask **to determine the optimized results**.

From the experimental data, the relationship between the mask aperture and the upper aperture of micro-tube **was** further analyzed to verify our assumption. As shown in **Fig. 5.8**, the size of upper aperture **varied** almost linearly with the mask aperture. This trend can be used to estimate for the size of mask aperture corresponding to the desired upper aperture. From this figure, it **was** apparent that the required size of mask

aperture was within the range from 6.7 $\mu\text{m}$  to 7.3 $\mu\text{m}$  because the desired upper aperture was 5 $\mu\text{m}$  in size. Therefore, the validity of the above method about mask design was verified.

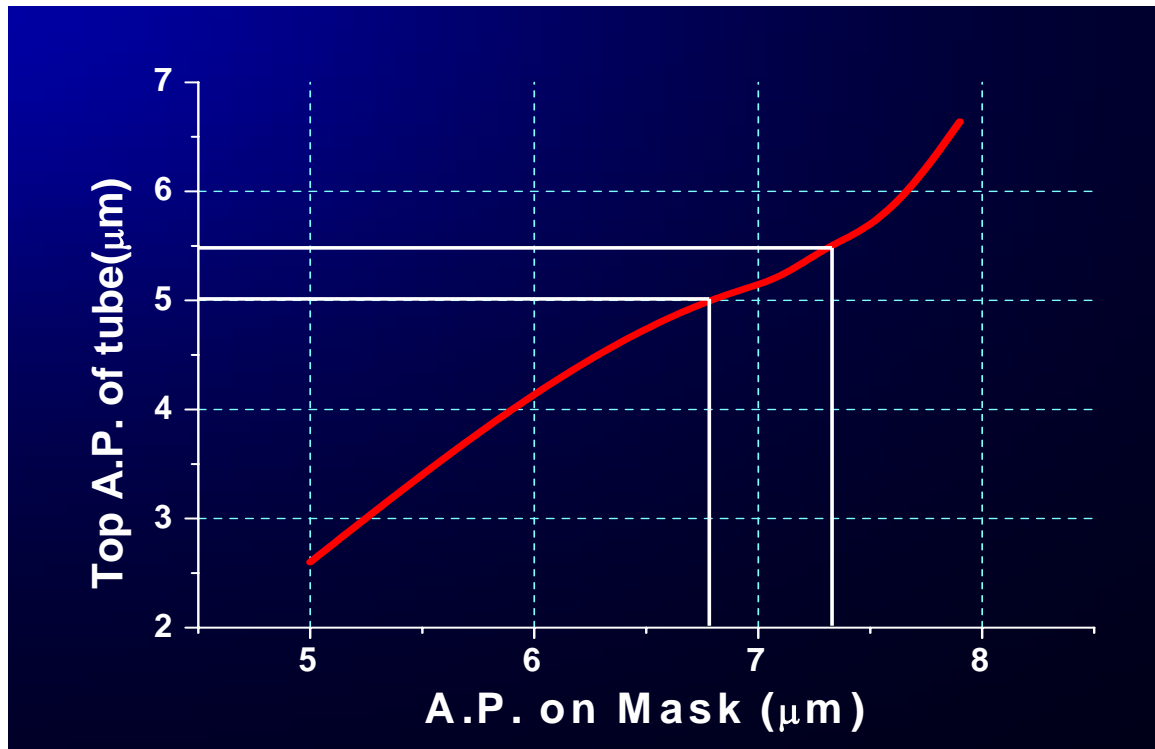


Fig. 5.8 Relationship between the upper aperture of tube and aperture size of the mask

Considering that the exposure time of the 1<sup>st</sup> mask was 7sec and its aperture was enlarged to 6.9 $\mu\text{m}$ , the fabricated structure was shown in Fig. 5.9. As demonstrated in this figure, the fabricated upper aperture was 5.1 $\mu\text{m}$  and the tube height maintained a desired value more than 2.5 $\mu\text{m}$ . However, it should also be noted that the tube was not covered with Al completely so that the real transmissive region for a micro-tube was not the upper aperture but the region surrounded with Al. A significant difference was observed between the upper aperture and the real transmissive region. Finally, as shown in Fig. 5.9, it was found that the Al did not cover over the sidewall completely and the tile angle was only 40 degrees. Therefore, some fabrication parameters must be still taken into account and they would be modified to solve the mentioned problem in the



micro-tube structure.

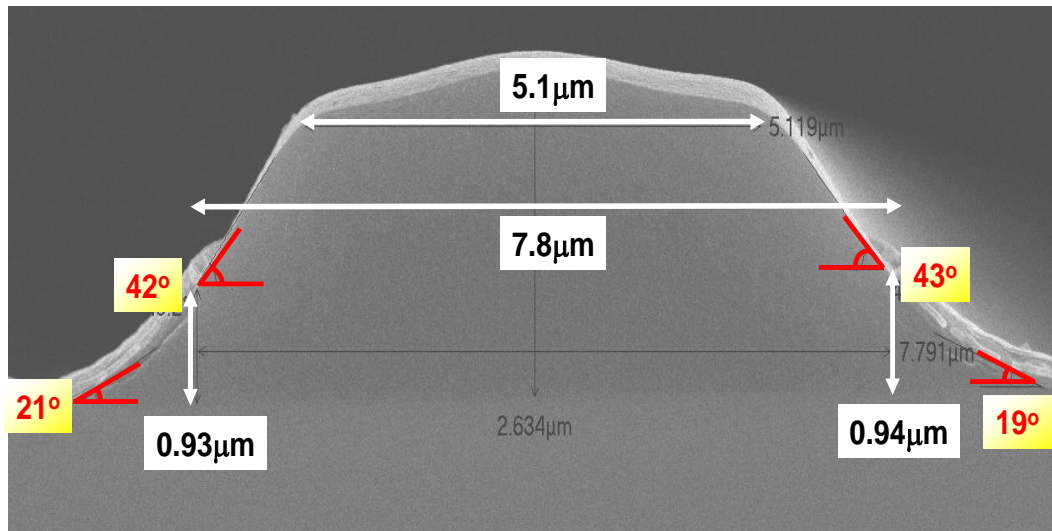
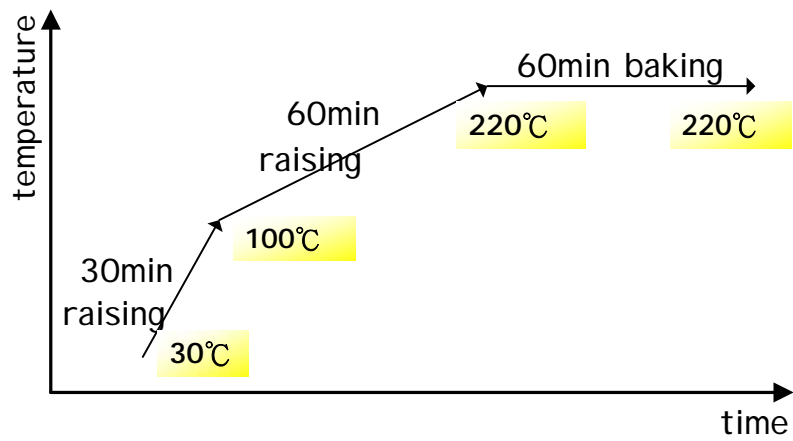


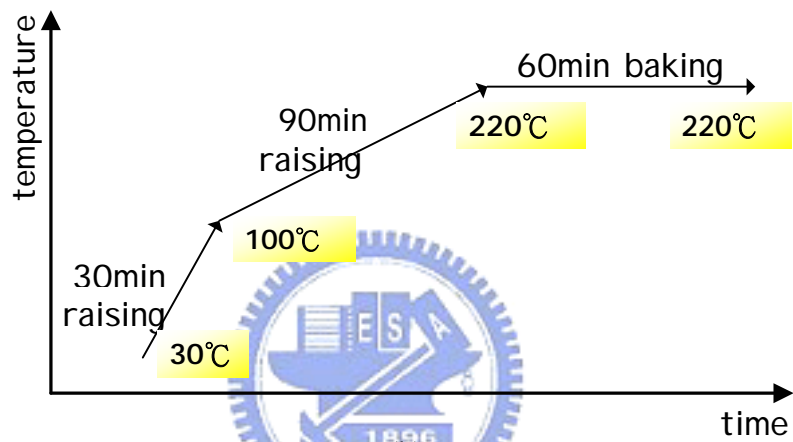
Fig. 5.9 A photograph of fabricated structure from SEM after mask aperture size was enlarged.

## 5.5 Tilt Angle

After considering the exposure time and aperture size of the 1<sup>st</sup> mask, the next fabrication parameter was temperature-rising curve of the oven, which included both temperature and time variables. According to the results from other experiments by using the general recipe, the tilt angle depended on the temperature-rising curve of the oven principally. Fig. 5.10(a) illustrated the default setting of the oven. Clearly visible in this figure was that the curve included two temperature-raising periods and one baking period. Herein, it is worth emphasizing that the temperature-raising period from 100°C to 120°C was the most critical factor of influencing on the tilt angle. Therefore, we proposed a new temperature-raising curve as shown in Fig. 5.10(b), in which the temperature-raising time from 100 to 220 was extended from 60min to 90min. Because of the time extension, there was enough time to take the desired shape and tilt angle. Micro-tubes could be protected from a serious reflowing process.



(a)



(b)

Fig. 5.10 Temperature-rising curve of the oven (a) the default setting (b) the modified setting of the oven

As shown in Fig. 5.11, it is apparent that the tile angles increase from 42° to 50°. This result agrees with the mentioned assumption that the second temperature-raising period is the most critical factor of influencing on the tile angle.

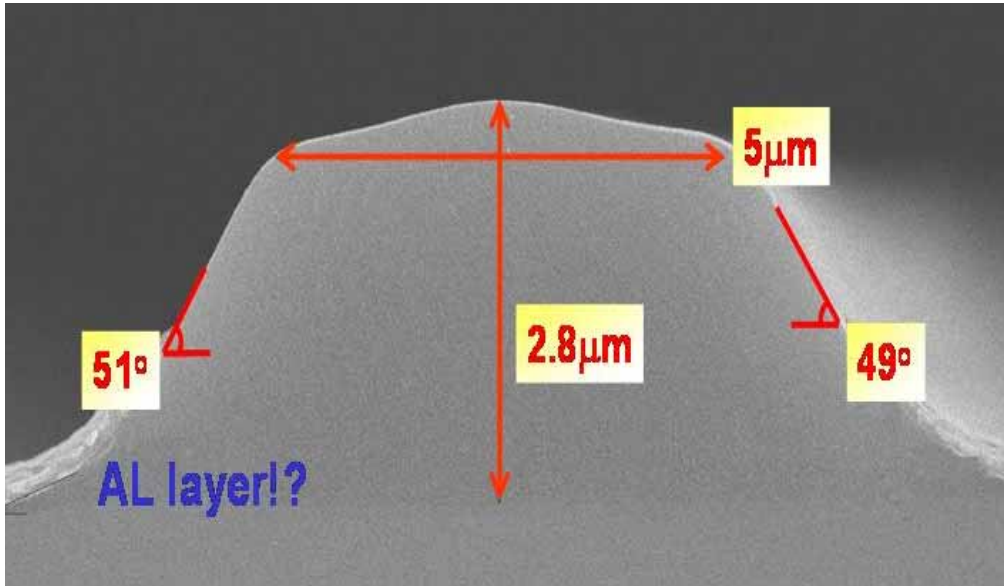


Fig. 5.11 A photograph of fabricated structure from SEM after temperature-rising curve was modified

A point to observe was that the tilt angle was still smaller than the optimized result of 60°. Therefore, we further proposed the third temperature-raising curve as shown in Fig. 5.12 and added an extra period, in which the temperature was kept at 110°C in 30min. Besides, the following temperature-raising time was still extended from 60min to 90min in compassion with the original recipe. Because of this extra temperature-holding period, there was more time to take the desired shape.

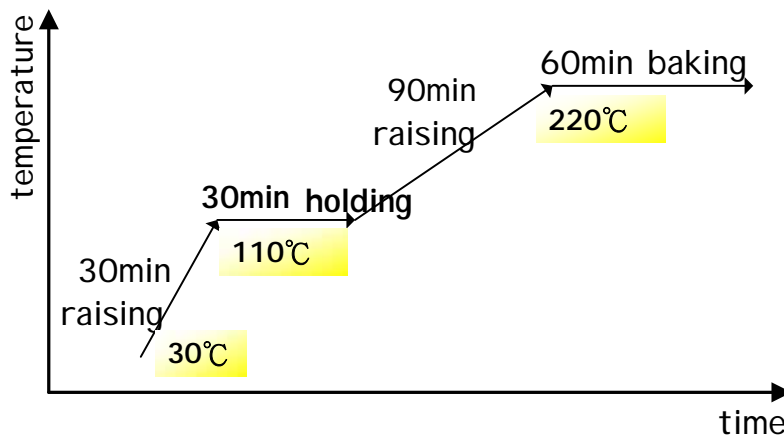


Fig. 5.12 Modified temperature-rising curve of the oven

The fabricated result was shown in Fig. 5.13. It would be clear from this figure that the tilt angle is almost  $60^\circ$  and this meets the requirement for the optimized structure.

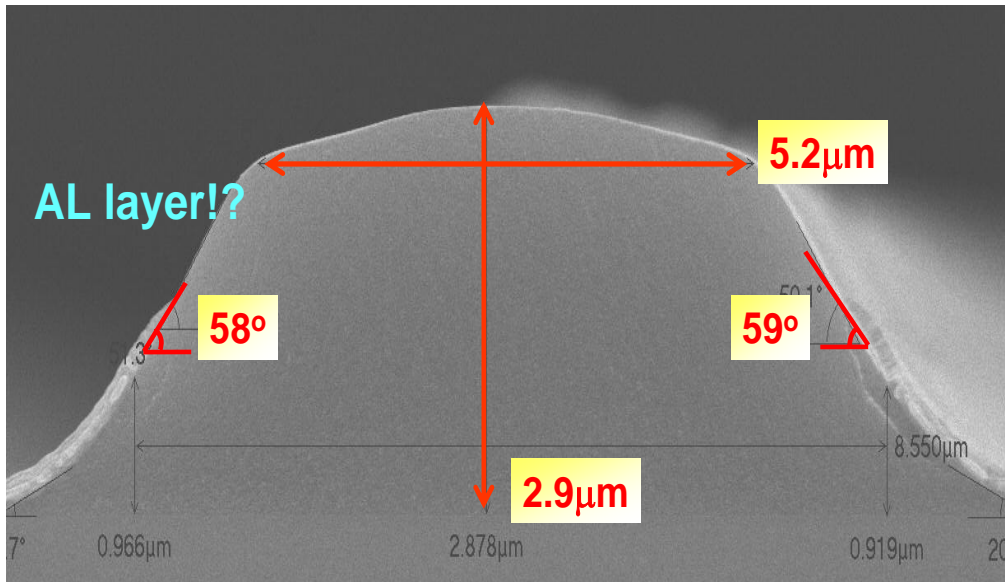


Fig. 5.13 A photograph of fabricated structure from SEM after the third temperature-rising curve was adopted.

Moreover, there **was** one further point that we must not ignore from Fig. 5.11 and Fig. 5.13. It **was** the fact that the tube **was** not covered with Al completely so that the real transmissive region for a micro-tube **was** not the upper aperture but the region surrounded with Al. The same observation **applied** to the 3-D picture from AFM in Fig. 5.14. This issue **deserved** explicit emphasis because the high-reflecting area covering on the tubes would be reduced significantly so that light efficiency enhancement was decreased.

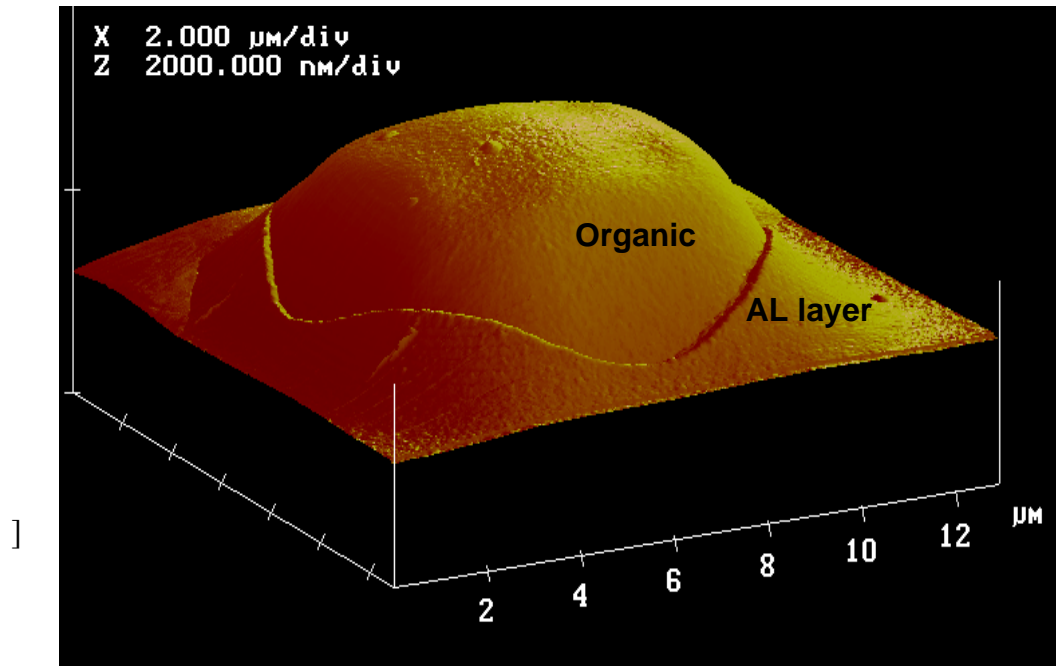


Fig. 5.14 A 3D AFM scan of the fabricated structure

## 5.6 Al Covering

Considering the influence of the 2<sup>nd</sup> mask exposure on Al-covering, we **proposed** the fourth fabrication factor to solve the mentioned problem. Because of the increased tilt angle and tube height, the positive photoresist covering above the Al layer would be thinner compared with the mentioned samples in the same fabrication. Besides, considering the diffraction effect in exposure, this would lead to the fact that more photoresist **were** removed so that the Al layer **did not** cover the tubes completely. A schematic explanation was given in **Fig. 5.15**.

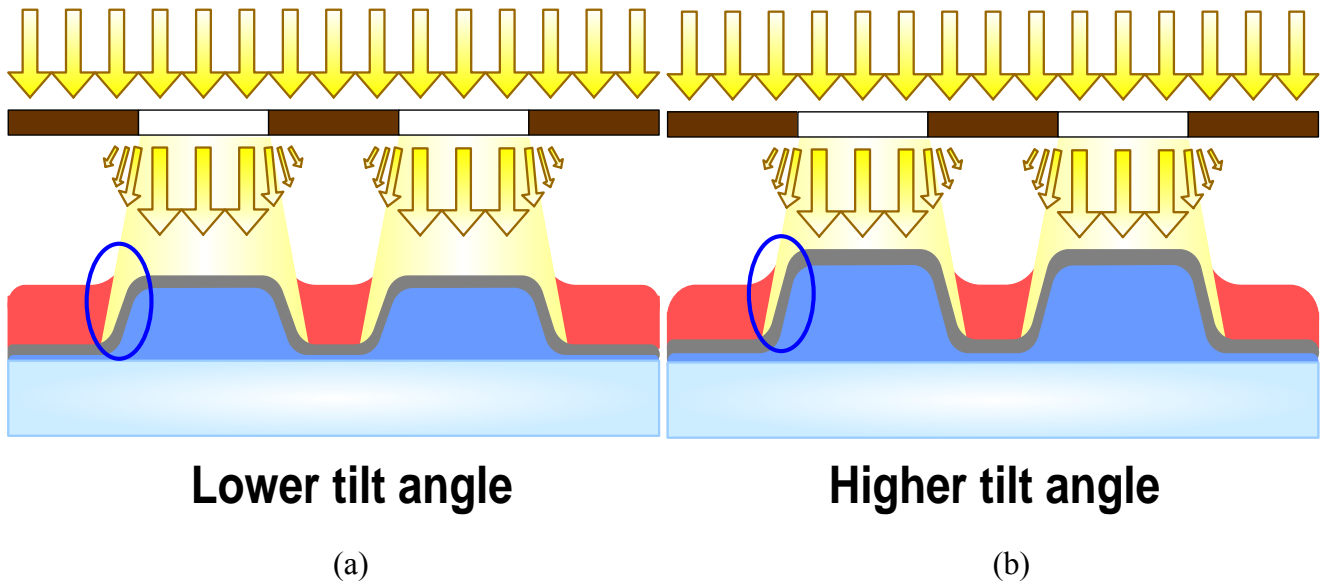


Fig. 5.15 Schematic of Al covering in fabrication for (a) lower and (b) higher tilt angle

The exposure time of the 2<sup>nd</sup> mask was reduced from 1.46sec to 0.3sec. Then, the fabricated structure was shown in Figs. 5.16 and 5.17. It was observed obviously that the tube was covered with the Al layer nearly so that the height of Al-covering can be more than 2.0 $\mu$ m. These two figures proved clearly that the Al-covering can be further heightened by reducing the exposure time of the 2<sup>nd</sup> mask.

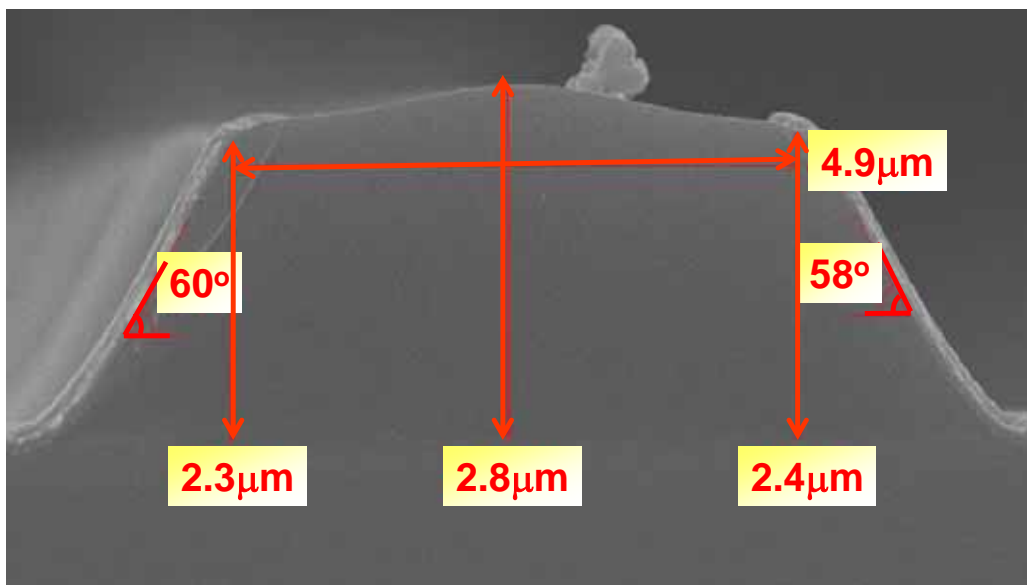


Fig. 5.16 A photograph of fabricated structure from SEM after the exposure time of the 2<sup>nd</sup> mask was reduced.

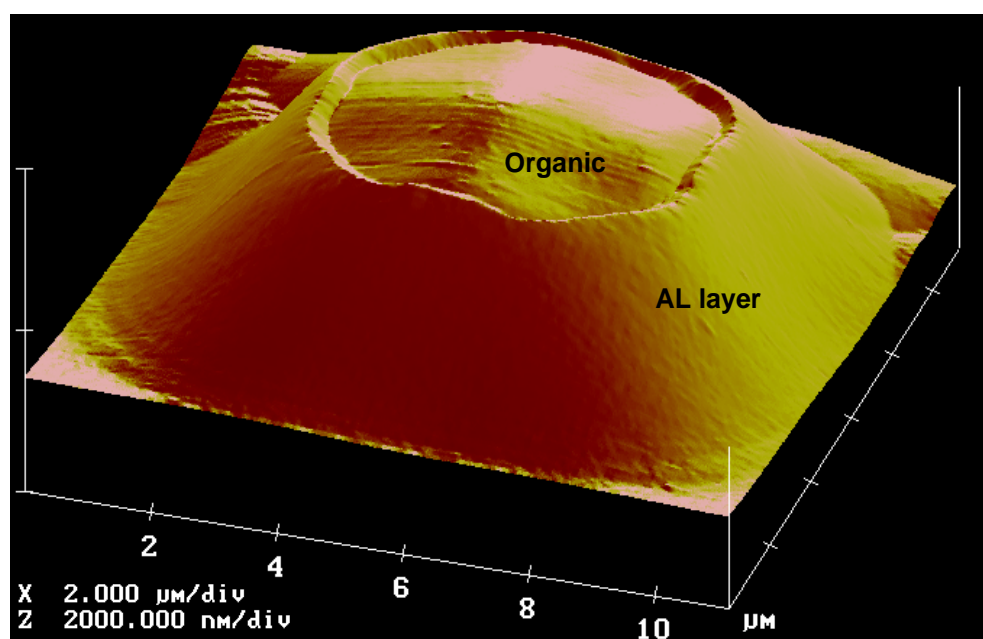


Fig. 5.17 A 3D AFM scan of the fabricated structure

## 5.7 Characterization

After the whole fabrication, an optical measurement system-ELDIM was utilized to measure the transmissive light utilization efficiency of micro-tube array structure for parallel backlight source. Because the material of micro-tube is organic layer of which the refractive index is about 1.5, this will result in the total internal reflection for backlight at large viewing angles and the decrease in the light efficiency enhancement. In order to solve this problem, three kinds of diffusers with 50% haze, 80% haze and 50% haze plus 80% haze were utilized. Herein, the fabricated micro-tube array was placed between two glasses so that the real situation can be simulated, and then the diffusers adhered to the surface of the upper glass.

The measured results were shown in Fig. 5.18. The measured data were utilized to plot a chart of the relationship between light efficiency enhancement and viewing angle. As shown in Fig. 5.18, a diffuser with higher haze value would result in higher light efficiency enhancement. This is very reasonable because a diffuser with higher haze

value **can** reduce the effect of total internal reflection effectively, which **made** more backlight reflected by the micro-tubes exit from upper apertures. Besides, clearly visible in the figure **was** that the highest light efficiency enhancement **appeared** at large viewing angles, which **can** be interpreted well by the fact that parallel backlight **would** be reflected by micro-tubes and then exit from upper apertures at  $60^\circ$  after the elimination of total internal reflection. Moreover, it **was** also worth noticing that there **was** high enhancement in the normal direction. This **was** because for backlight at various incident angles the superimposition of light intensity **would** be more noticeable in the normal direction than in other directions. Finally, the measured enhancement **was** a factor of 1.81 and this **showed** an agreement between simulated results and experiment, implying that the simulated enhancement for the optimized structure **was** about a factor of 2.0 and this **approximated** to the measured value. However, strictly speaking, the little difference can be interpreted well by the fact that the fabricated structure **was** not still optimized, in which the upper aperture **was** a little larger and the tube **was** a little shorter compared with the optimized structure. Besides, there **was** smaller tilt angle in the position nearer to the bottom of a tube. Moreover, we must also consider some factors, which **resulted** in light loss, such as total internal reflection and the absorption of the materials, etc. Finally, from the measured results it can be concluded that the micro-tube array with high light efficiency enhancement of a factor of 1.81 can certainly collect backlight effectively and enhance backlight utilization efficiency.



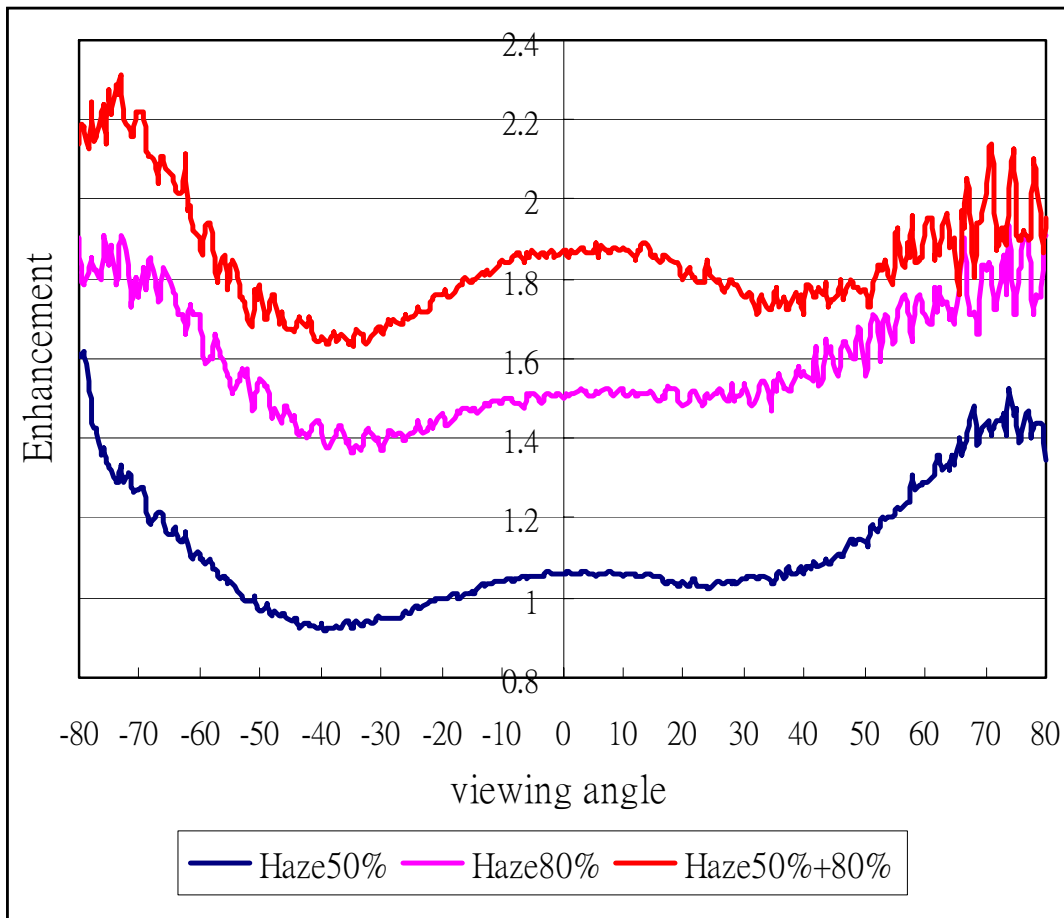


Fig. 5.18 Relationship between light efficiency enhancement and viewing angle for diffusers with different haze values.

# Chapter 6

## Application

### 6.1 Introduction

For conventional transflective LCDs, the design of the light scattering property is very important for the reflective region since it determines how effectively reflective light is transferred to the direction of the eyes.

It is necessary to design the light scattering property of incident light suitably in order to produce a clear view of image. When characters are written on the mirror, the characters are not seen easily because the images of fluorescent light or our own faces reflect and hinder the view. On the other hand, excessive scattering reduces a light intensity per solid angle and decreases brightness. Therefore, optimum control of the scattering characteristic is required to produce clear and bright image on a display.

### 6.2 Bump Reflector

While several structures are considered to realize the light scattering property for conventional transflective LCDs, at present a structure that has micro bumps on its surface (micro reflective structure = MRS) [26] has been adopted. This structure allows the bright image with high aperture ratio and no double image attributed to the parallax. [27]- [30]

As discussed above, a method to estimate and design a reflector for the reflective region in conventional transflective LCDs has been developed. This method is based on the assumption that the surface shape of bumps on the reflector could be practically replaces with a set of multiple micro-flat mirrors as shown in Fig. 6-1.

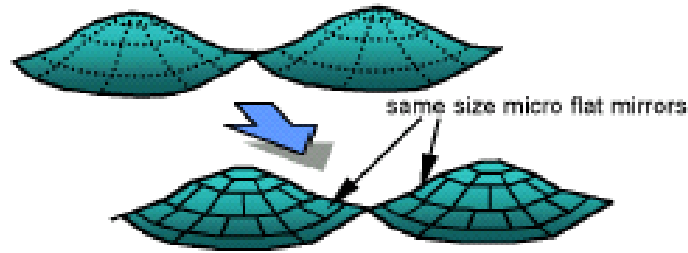


Fig. 6.1 Schematic figure of bump reflector composed by many micro flat mirrors

And then, a required slope angle distribution for an ideal reflector could be calculated as shown in Fig. 6-2. Thus, it is understood that the ideal slope angle distribution of the reflector is; there is little flat part, the existence rate increases up to 8° but no larger slope angle than this exists.

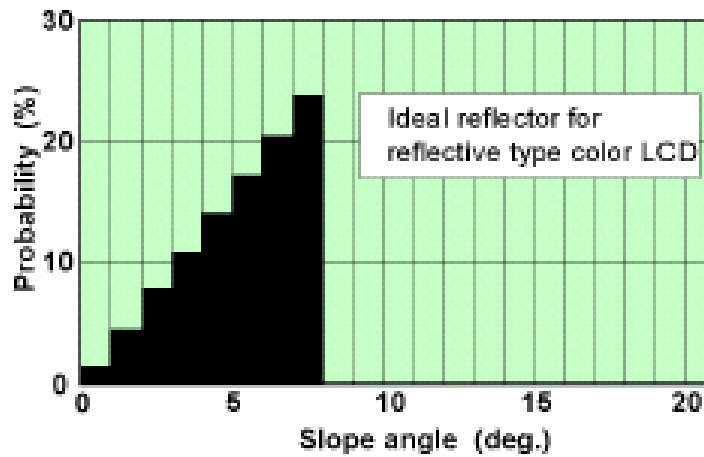


Fig. 6.2 Slope angle distribution of an ideal reflector

### 6.3 Concave Reflector

For the bump reflector in conventional transfective LCDs, the fabrication process includes the alignment and exposure of two masks and the following reflow process. Although this is a typical TFT-LCD process, there might still be some fabrication considerations. Herein, there might be an alignment error because two masks were required. Moreover, it is necessary to control some fabrication parameters in the reflow process to obtain a required height and slope angle distribution, which might result in great complexity in the fabrication. Therefore, in order to simplify the fabrication process for the reflective region and increase the light utilization efficiency of backlight

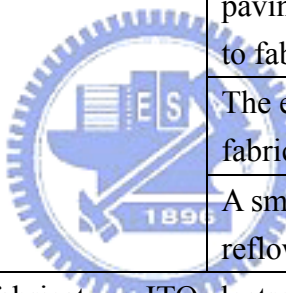
in conventional transfective LCDs, we further proposed a novel reflector structure-concave reflector built above the micro-tube array so that the whole image quality and brightness can be improved for both indoor and outdoor application.

During the reflective mode in transfective LCDs, the concave reflector can be utilized to reflect the ambient light to perform display efficiently as the bump reflector. The concave reflector is similar to a semicircle cave in shape and can be fabricated in the regions among the micro-tubes, which was unavailable before. This is a novel method to fabricate the reflective region and make conventional fabrication process be further simplified. First, some organic material would be spun coating on the micro-tube array and this can result in a structure with wave shape, in which the concave region will be taken as the reflector. Above the organic layer, there are an ITO electrode, a Molybdenum (MOLY) layer [31] and an Al layer in turn. As long as spin-coating speed and time of organic layer was controlled appropriately, we can fabricate a concave reflector with slope angle distribution similar to the bump structure. The difference between them is that one reflector is concave and the other is convex in shape. Therefore, it can be concluded that the concave reflector has a light scattering property similar to the bump reflector and a simplified fabrication compared to the bump reflector.

#### **6.4 Comparison**

A comparison between the fabrication processes of concave and bump reflectors would be given in Table. 6.1 and a flow chart of fabrication process for concave reflector is shown in Fig. 6.3.

Table. 6.1 Comparison between the concave reflector and bump reflector

Structure	Concave reflector	Bump reflector
Step 0	Micro-tube array had been fabricated.	Micro-tube array had been fabricated.
Step 1	An organic layer was spun coating on the Al layer. By controlling spin-coating speed and time appropriately, a desired wave-shaped structure can be fabricated.	A photoresist payer was spun coating on the Al layer.
Step 2	The exposure of the 2 <sup>nd</sup> mask, development and etching processes were utilized to keep the organic layer above upper apertures released.	The exposure of the 2 <sup>nd</sup> mask, development and etching processes were utilized to keep the photoresist layer above upper apertures released.
Step 3	An Al acid was utilized to remove the Al layer above upper apertures.	
Step 4		An organic layer was spun coating to be a paving layer.
Step 5		Another organic layer was spun coating on the paving layer. The exposure of a mask was utilized to fabricate a one-step structure.
Step 6		The exposure of another mask was utilized to fabricate a four-step structure.
Step 7		A smooth bump structure was fabricated by the reflowing in an oven.
Step 8		An extra mask was utilized to fabricate an ITO electrode layer. Then, a MOLY layer was spun coating and an Al layer was sputtered in turn above the upper apertures.
Step 9	The structure was covered by spin coating a positive photoresist.	
Step 10	The exposure of the 2 <sup>nd</sup> mask, development and etching processes were utilized to keep the positive photoresist above upper apertures released.	
Step 11	Etching solutions were utilized to take away the Al and MOLY layers above the upper apertures, therefore only ITO electrode was kept.	
Step 12	The rest of positive photoresist was removed, and then liquid crystal was poured into this structure. Finally, a single-cell gap structure with a concave reflector can be fabricated.	

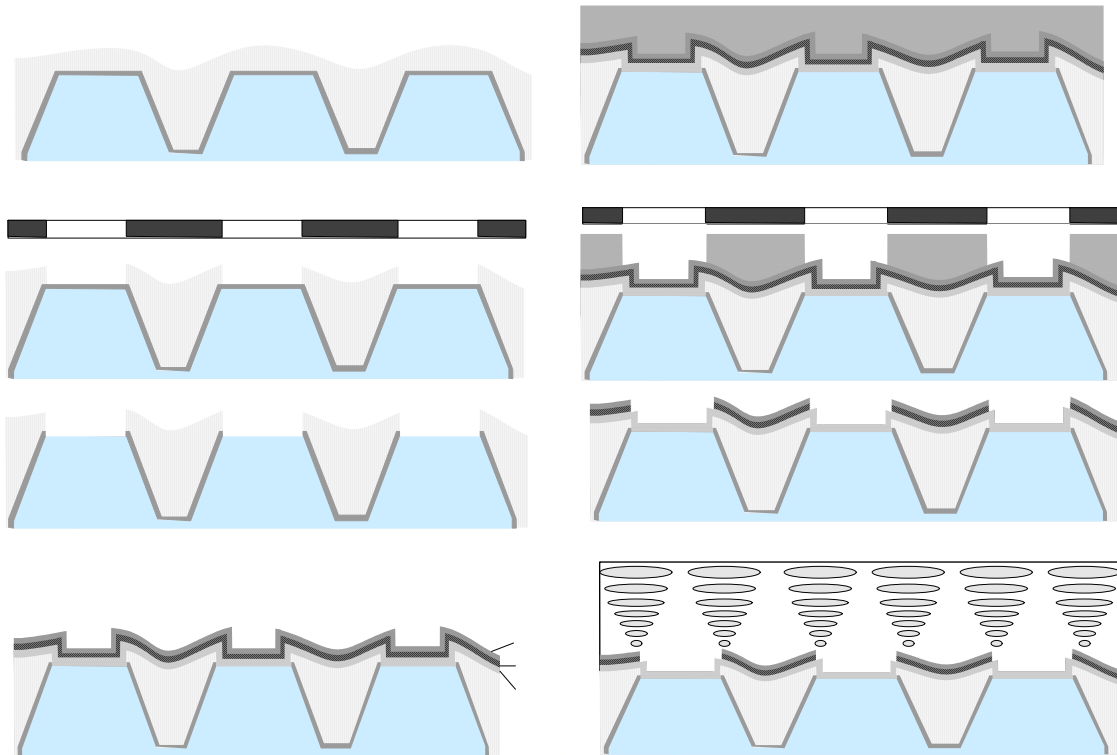


Fig. 6.3 Flow chart of fabrication process for concave reflector.

(1) Organic coating (2) UV exposure (3) Al etching (8) ITO and Moly coating, Al sputtering (9) photoresist coating (10) UV exposure (11) photoresist etching, and (12) LC pouring and the fabricated structure

Both of the reflectors were fabricated on micro-tube array, and then a comparison would be given in the same situation. From this table, it is apparent that in the fabrication process of concave reflector it does not need the procedures from step4 to step7, in which two masks were utilized in the fabrication process of bump reflector, and this would result in an alignment error. Besides, in step 7 an extra reflow process was necessary for a desired bump-shaped structure, which means that it needs more time and more complex processes to fabricate the bump reflector. Thus, the concave reflector is superior to the bump one according to the above table and discussion.

# Chapter 7

## Conclusions

### 7.1 Conclusion

With the population of internet and wireless communication, transfective LCDs become an important display technology. Light weight, high brightness, high resolution, high readability and good color saturation are major concerns. Several configurations have been proposed for the transfective LCDs technology, however, they suffer from the low aperture ratio, low light utilization, slow response time, and different color saturation, etc. In order to solve the problem about low light utilization, a novel transfective LCD with micro-tube array was proposed to make most backlight pass through the panel, yielding high transmissive light utilization efficiency. Besides, the area ratio of the transmissive region to the reflective one can be redistributed so that backlight and ambient light can both be utilized effectively. All properties of our design mentioned above should be characterized, therefore, a preliminary embodiment was designed and experimented to confirm the light utilization efficiency and light distribution. A typical TFT-LCD process was utilized to carry out the micro-tube array structure due to its convenient and cost-effective manufacturing process. Finally, the measurement instruments were utilized to characterize the properties of the fabricated structure and compared with simulation results.

From the simulation results, we designed and optimized the micro-tube array structure by varying the size of upper aperture, the tube height, and tile angle. Besides, different backlight sources were utilized to verify its generalization. Based on the fabrication limitations, we chose the micro-tube array with the specifications of  $d=3\mu\text{m}$ ,

$\theta_{\text{tube}}=60^\circ$  and  $AP=5\mu\text{m}$  for the applications. Moreover, various aperture shapes used to optimize our design were also presented. After that, we compared the simulated structure with micro-tube array to conventional structure, and then a significant light efficiency enhancement can be obtained. As a result, from this viewpoint, one may say that a novel transfective structure with the micro-tube array has a distinguished capability for the collecting of light compared with traditional transfective structure.

In the following experiment, considering the priority of fabrication processes, there are four key factors determining the partial structures of a single micro-tube respectively. At first, considering the tube height, the exposure time of the 1<sup>st</sup> mask played a leading role. By shortening the exposure time, the influence of diffraction effect on the structure could be decreased effectively. The tube height can be optimized and larger than  $2.5\mu\text{m}$  with the decrease of exposure time from 20sec to 7 sec. The second issue was relative to the aperture size of mask. The size of upper aperture increased almost linearly with the mask aperture. Therefore, the required aperture size of mask was within the range from  $6.7\mu\text{m}$  to  $7.3\mu\text{m}$  because the desired upper aperture was  $5\mu\text{m}$  in size. After considering the exposure time and aperture size of the 1<sup>st</sup> mask, the next fabrication factor was temperature-rising curve of the oven, which included both temperature and time variables. Herein, the tilt angle depended on the temperature-rising curve of the oven principally. After the recipes were modified, it would be clear from the fabricated result that the tilt angle is almost  $60^\circ$  and this met the requirement for the optimized structure. Finally, we considered the influence of the 2<sup>nd</sup> mask exposure on Al-covering, and then reduced the exposure time of the 2<sup>nd</sup> mask from 1.46sec to 0.7sec. The fabricated structure showed that the tube was covered with the Al layer completely so that the height of Al-covering can be of more than  $2.0\mu\text{m}$ . After the whole fabrication, the optimized structure was obtained.



An optical measurement system-ELDIM **was** utilized to measure the transmissive light utilization efficiency of micro-tube array structure for parallel backlight source. The measured enhancement **was** a factor of 1.81, agreed with simulated results and experiment, implying that the simulated enhancement for the optimized structure **was** about a factor of 2.0 close to the measured value. Thus, it can be concluded that the micro-tube array with high light efficiency enhancement can certainly collect backlight effectively and enhance backlight utilization efficiency.



# Reference

- [1] E. Lawrence, and J. Tannas, Flat-Panel Displays and CRTs, Van Nostrand Reinhold, New York (1995).
- [2] A. R. Kmetz, A single polarizer twisted nematic display, Proc. SID 21, 63 (1980).
- [3] S. T. Wu, and D. K. Yang, Reflective Liquid Crystal Displays (Wiley, 1998).
- [4] H. J. Cornelissen, M. Ouwerkerk, and P. A. Duine, Transflective Display Device, U.S. patent 6437900 B1 (2000).
- [5] M. Kubo, Y. Narutaki, S. Fujioka, Y. Maruyama, S. Takayuki, Y. Yoshimura, M. Katayama, Y. Ishii, S. Yamakawa, Ban, and Atsushi, LCD with plurality of pixels having reflective and transmissive regions, U.S. patent 6295109 B1 (1998).
- [6] T.M. David, et al., WO patent 0017707 (2000).
- [7] M. Okamoto, H. Hiraki, and S. Mitsui, Liquid Crystal Display, U.S. patent 6281952 B1 (1998).
- [8] M. Jisaki, and H. Yamaguchi, IDW'01, p. 133 (2001).
- [9] S. Takeuchi, Liquid Crystal Display Device, U.S. patent 6734942 (1998).
- [10] P. Yeh, and C. Gu, Optics of Liquid Crystal Displays (Wiley, 1999), p.252.
- [11] M. Born, and E. Wolf, Principle of Optics (Pergamon Press, New York, 1998).
- [12] S. T. Wu, and D. K. Yang, Reflective Liquid Crystal Displays, p. 98-108 (Wiley, 1998).
- [13] P. Yeh, and C. Gu, Optics of Liquid Crustal Displays, p.222-224 (Wiley, 1999).
- [14] E. Jakeman and E. P. Raynes, Electro-optic response times of liquid crystal, Phys. Lett. A39, 69 (1972).
- [15] I. C. Khoo and S. T. Wu, "Optics and Nonlinear Optics of Liquid Crystals" (World Scientific, Singapore, 1993).
- [16] Ricci, Robert W., Mauri A. Ditzler, and Lisa P. Nestor, Discovering the

- Beer-Lambert Law, *J. of Chemical Education* 71, 983-985, 1994.
- [17] Lykos, and Peter, The Beer-Lambert Law Revisited: A Development without Calculus, *J. of Chemical Education* 69, 730-732, 1992.
- [18] K. H. Fan Chiang, S. T. Wu, and S. H. Chen, Fringing Field Effect of Liquid-Crystal-on-Silicon Devices, *Jpn. J. Appl. Phys. Vol. 41*, pp. 4577-4585 (2002).
- [19] M. B. Stern, M. Holz, S. S. Medeiros and R. E. Knowlden, Fabricating binary optics: Process variables critical to optical efficiency, *J. Vac. Sci. Technol. B9*, 3117 (1991).
- [20] W. Daschner, P. Log, Michael Larsson and S. H. Lee, Fabricating of diffractive optical elements using a single optical exposure with a gray level mask, *J. Vac. Sci. Technol. B13*, 2729 (1995).
- [21] T. J. Suleski, and D. C. O'shea, Gray scale mask for diffractive-optics fabrication: I. Commercial slide imagers, *Appl. Opt.* 34, 627 (1995).
- [22] P. Sixt, J. M. Stauffer, J. M. Mayer, P. Regnault, and G. Vorin, One-step 3S shaping using a gray-tone mask for optical and microelectronic applications, *Microelectron. Eng.* 23, 449 (1994).
- [23] J. W. Goodman, *Introduction to Fourier Optics*, Wiley, New York (1985).
- [24] W. Henke, W. Hoppe, H. J. Quenzer, P. Staudt-Fischbach, and B. Wranger, Simulation and Experimental study of gray-tone lithography for the fabrication of arbitrary shaped surfaces, *Proc. IEEE Micro Electro Mechanical Syst.*, pp. 205-210 (1994).
- [25] E. C. Harvey, P. T. Rumsby, M. C. Gower, and J. L. remnant, Microstructuring by excimer laser, *Proc. SPIE*, 2639, pp. 266-277 (1995).
- [26] Suzuki, Kenkichi; Matsuda, Masaaki; Hayashi, Nobuaki, Polymer resist materials for excimer laser ablation lithography, *Applied Surface Science* 127-129, pp.

905-910 (1998).

- [27] S. Y. Kim, S.Y. Ryu, J. M. Choi, S. J. Kang, S. P. Park, S. Im, C. N. Whang, and D. S. Choi, Characterization and luminescence properties of Alq3 films grown by ionized-cluster-beam deposition, neutral-cluster beam deposition and thermal evaporation, *Thin Solid Films*, 78-81, pp. 398-399 (2001).
- [28] S. Cobb, and Jr., Totally internally reflecting thin, flexible film, U.S. patent 4906070 B1 (1988).
- [29] S. Cobb, and Jr., Totally internally reflecting thin, flexible film, U.S. patent 5056892 B1 (1991).
- [30] F. J. Ko, and H. P. D. Shieh, *Jpn. J. Appl. Phys.* 39, pp. 2647 (2000).
- [31] Y. P. Huang, J. J. Chen, F. J. Ko, and H. P. David Shieh, Multidirectional Asymmetrical Microlens Array Light Control Film for Improved Image in Reflective Color Liquid Crystal Displays, *Jpn. J. Appl. Phys.* Vol. 41, pp. 646-651 (2002).
- [32] D-L. Ting, W-C. Chang, C-Y. Liu, J-W. Shiu, C-J. Wen, C-h. Wen, C. H. Chao, L-S. Chuang, C-C. Chang, A High-Brightness High-Contrast Reflective LCD with a Micro Slant Reflector (MSR), *SID 99 Digest*, vol. 45, p. 954 (1999).
- [33] T. Uchida, T. Nakayama, T. Miyashita, and T. Ishinaba, *Asia Display'95, Proc. 15<sup>th</sup> Int. Display Research Conf. (IDRC)*, Hamamatsu, Japan, p. 599 (1995).